Journal of Geochemical Exploration 199 (2019) 75–89

Contents lists available at ScienceDirect

Journal of Geochemical Exploration

journal homepage: www.elsevier.com/locate/gexplo

Early Jurassic magmatism and metallogeny in the Yizuomao area, Lesser Xing'an Range-Zhangguangcai Range, NE China: Evidence from petrogeochemistry, zircon U–Pb ages, and Hf isotopes

Shi-Jiong Han[a], Yan-Chen Yang[a,*], Bao-Yi Li[a], Vadim G. Khomich[b,c], Ji-Yao Wang[d], Qing-Lei Wang[e]

[a] College of Earth Sciences, Jilin University, Changchun, China
[b] Far East Geological Institute, Far Eastern Branch of Russian Academy of Sciences, Vladivostok, Russia
[c] School of Engineering, Far Eastern Federal University, Vladivostok, Russia
[d] Changchun Gold Research Institute, China
[e] Shanghai Municipal Engineering Design Institute (Group) Co., Ltd., China

ARTICLE INFO

Keywords:
Zircon U–Pb dating
Zircon Hf isotopes
Geochemistry
Yizuomao Complex
Eastern Ha'erbin
Heilongjiang

ABSTRACT

The Yizuomao area, located in the south segment of Lesser Xing'an Range–Zhangguangcai Range, is an important part of ore-concentrated area in the east of Ha'erbin. The Yizuomao Complex comprises medium- to coarse-grained, medium- to fine-grained and fine-grained biotite-bearing alkali feldspar granite, and the results show $^{206}Pb/^{238}U$ ages of 195.3 ± 1.8 Ma, 200.6 ± 3.2 Ma and 205.2 ± 4.1 Ma, respectively. The geological characteristics for these deposits indicate that a genetic link between the emplacement of granite porphyries and skarn-type mineralization. The ages of regional mineralization and crystallization of the granite porphyrie suggest that skarn mineralization in the Yizuomao area occurred during the late Early–early Middle Jurassic. The Yizuomao Complex and associated granite porphyries have similar characteristics, as both comprise high–K calc–alkaline rocks containing high concentrations of SiO_2 and $K_2O + Na_2O$, and low concentrations of Ti, Fe, Mn and Ca. The magmatic rocks are depleted in Ba, Nb, Sr, and Ti, and enriched in Rb, Th, U, K and Pb, and have high Rb/Sr ratios, characteristic of highly fractionated I-type granites. Moreover, all display positive $\varepsilon_{Hf}(t)$ values from +5.6 to +14.3, and young zircon Hf single-stage and two-stage model ages, suggesting a significant contribution of juvenile material. Based on the geochronology, geochemistry and Hf isotopic data, we suggest that the Yizuomao Complex and associated granite porphyries were derived from partial melting of juvenile crust. The Yizuomao Complex was emplaced in the transformation period from the post-collision extension of the NCC and the Jiamusi-Khanka Massif to the subduction of Paleo-Pacific Plate. The granite porphyries that are intimately associated with the mineralization were the result of magmatic activity along an active continental margin related to subduction of the Paleo-Pacific Plate.

1. Introduction

The Central Asian Orogenic Belt (CAOB) is one of the largest and most complex Phanerozoic accretionary orogens on Earth (Sengör et al., 1993; Windley et al., 1984), extending for > 5500 km from the European craton in the west to the Pacific Ocean in the east (Fig. 1a). The Lesser Xing'an Range–Zhangguangcai Range is located in the eastern segment of the CAOB, between the North China craton (NCC) and Siberia Craton, and is bordered by the Mudanjiang Fault to the east and the Heihe–Nenjiang–Hegenshan Fault to the north (Fig. 1b). Formation of the metallogenic belt was related to terminal closure of the Paleo-Asian Ocean and amalgamation of micro-continental blocks during the Paleozoic (Jahn et al., 2004; Li, 2006; Li et al., 1999; Sengör et al., 1993; Xiao et al., 2009), along with Mesozoic overprinting of the region by the Mongol-Okhotsk tectonic realm in the northwest and the Paleo-Pacific tectonic realm in the east (Li et al., 1999; Wu et al., 2007a; Xu et al., 2013; Zhou et al., 2014), which led to extensive magmatism. In recent years, mineral deposits have been discovered in the Lesser Xing'an Range–Zhangguangcai Range, including the Daheishan Mo deposit (Zhang, 2013), Cuihongshan W-Mo-Zn polymetallic deposit (Yang et al., 2012), Huojihe Mo deposit (Han et al., 2012), Luming Mo deposit (Han et al., 2012), Dong'an Au deposit (Han, 2013), Tuanjiegou

* Corresponding author at: 2199 Jianshe Street, College of Earth Sciences, Jilin University, Changchun 130061, China.
E-mail address: yyc@jlu.edu.cn (Y.-C. Yang).

https://doi.org/10.1016/j.gexplo.2019.01.009
Received 15 March 2018; Accepted 23 January 2019
Available online 26 January 2019
0375-6742/

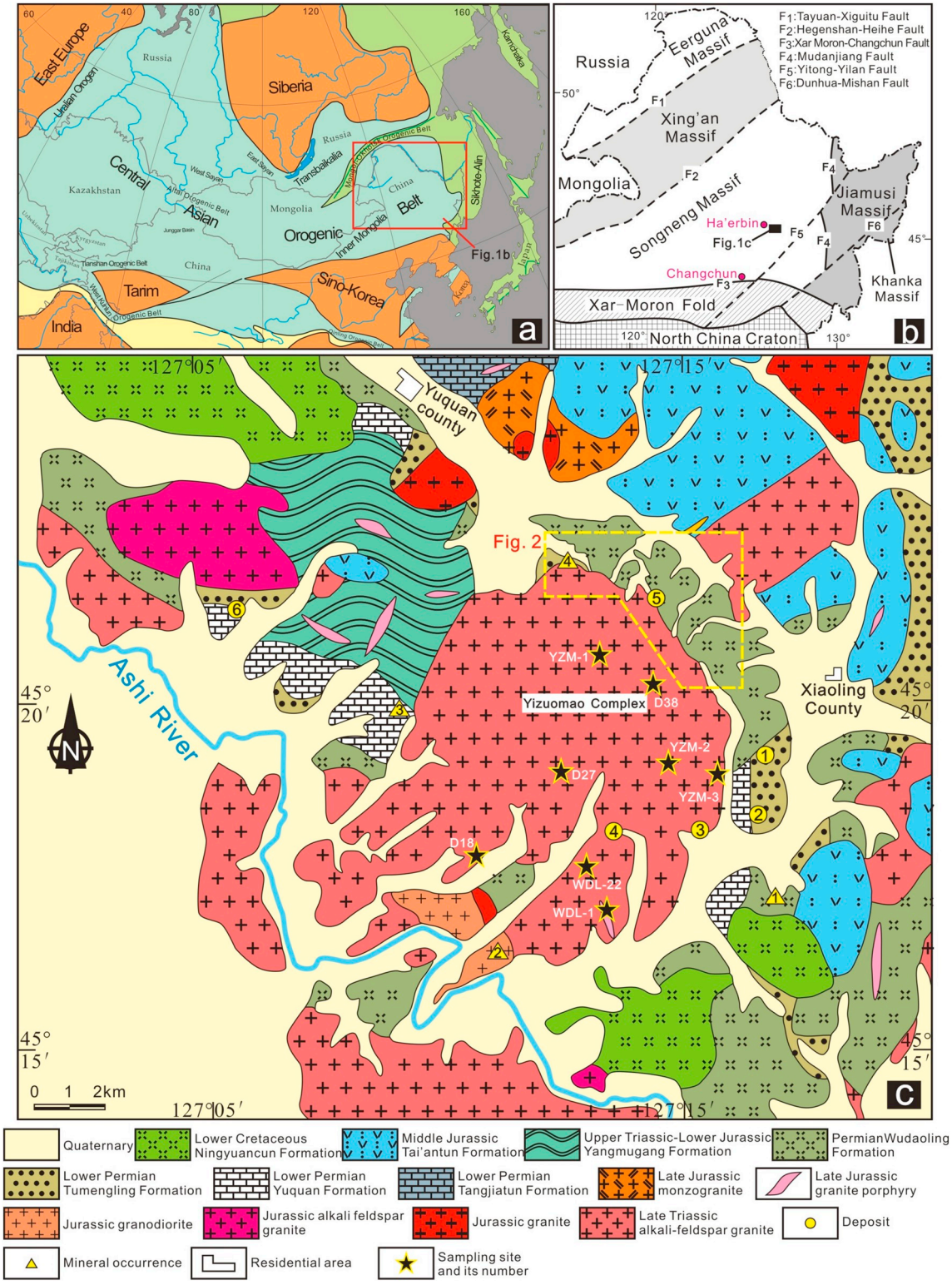

Fig. 1. (a) Geotectonic map of China and adjacent regions; (b) geotectonic division map of northeastern (NE) China; (c) regional geological map of the Yizuomao area. Deposits: 1—Sujiaweizi Fe-Zn; 2—Shifa Fe-Zn; 3—Erdaoling Pb-Zn; 4—Wudaoling Fe-Mo; 5—Bailing Cu-Zn; 6—Zhangjiawan Fe–Zn. Mineral occurrences: 1—Nantaizi Fe; 2—Xiaohekou Fe-Cu; 3—Tianchengyao Fe; 4—Yizuomao Cu.

Au deposit (Sun et al., 2012a, 2012b), Xiaoxilin Pb–Zn deposit (Tan, 2009). As such, this area represents an important source of noble and non-ferrous metals in northeast China.

The Yizuomao Complex is located in the south segment of Lesser Xing'an Range–Zhangguangcai Range and is associated with Fe, Cu, Zn, Pb and Mo polymetallic deposits (Fig. 1c). However, more detailed geochemical, geochronological, and petrological studies on the Yizuomao Complex and associated mineralization are required to better understand its formation and evolution. Previous studies, mostly published in Chinese by our research team, have focused on ore deposits around the Yizuomao Complex, such as the Bailing Cu–Zn deposit (Bo et al., 2016), the Sujiaweizi Fe polymetallic deposit (Li et al., 2015) and

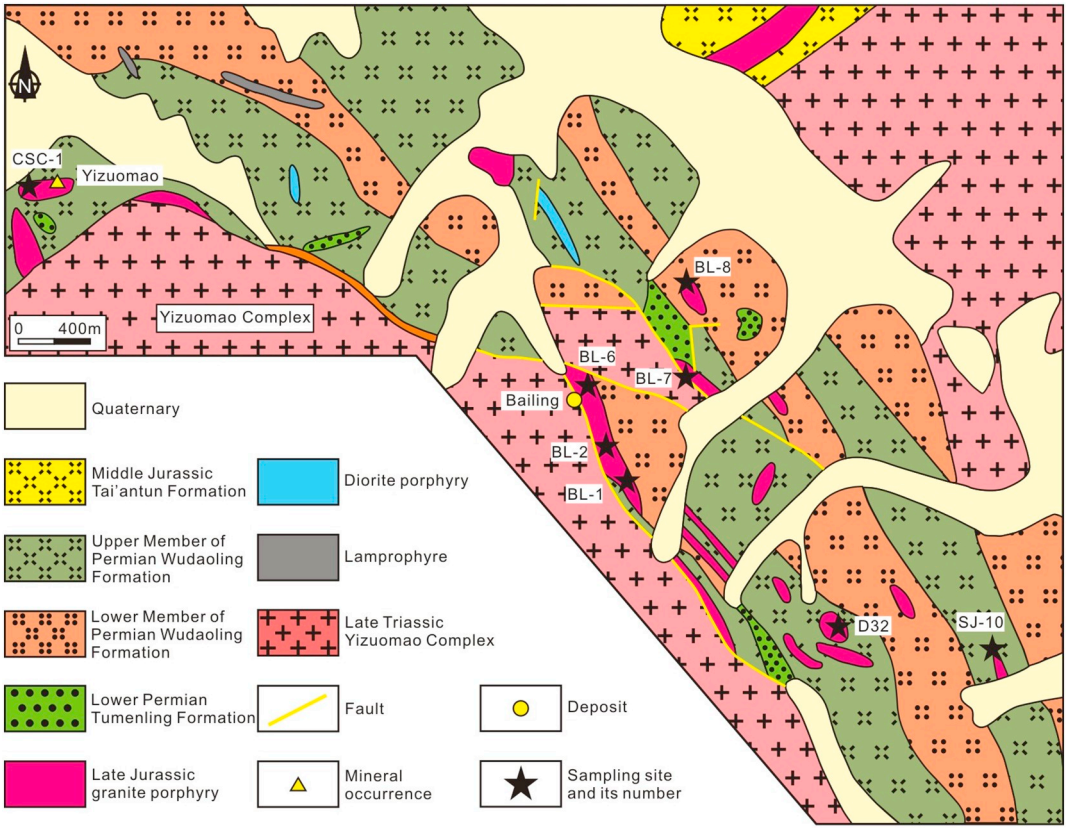

Fig. 2. Detailed geological map of the contact zone between the Yizuomao Complex and Wudaoling Formation.

the Wudaoling Mo–Fe deposit (Shi et al., 2012). These studies suggested a genetic link between the Yizuomao Complex and mineralization (Yang et al., 2007; Yan and Yang, 2008). However, a lack of any systematic geochemical and geochronological study of the Yizuomao Complex and the granite porphyry hinders our understanding of their genesis and relationship to skarn mineralization. Here we present the results of zircon U–Pb dating and whole-rock geochemistry analyses for the Yizuomao Complex and granite porphyry. The data constrain the petrogenesis of the Yizuomao Complex, the timing of skarn mineralization, and the broader tectonic setting at the time of magmatism and mineralization.

2. Geological background

The study area is located between the eastern margin of the Songliao Basin and the western margin of Zhangguangcai Range, and is an important part of ore-concentrated area in the east of Ha'erbin (Fig. 1c). The evolution of the region was characterized by several stages of magmatism, which provided favourable conditions for ore formation.

The Yizuomao Complex occupies an area of ~80 km^2 and has an irregular shape, with an outcrop length of ~10 km and width of ~8 km (Fig. 1c). Previous studies have indicated that the complex records magma emplacement spanning the Early to Middle Jurassic (161–164 Ma; Compiling Group, 1983; 180.9 Ma, Zhao, 2000) to the Late Triassic (218 Ma; Compiling Group, 1983; 224 Ma, Li and Zhao, 1991), with a diagenetic age mainly within the Early Yanshanian. The Yizuomao Complex can be subdivided into three phases and occurred as concentric ring. The internal phase is composed mainly of coarse-grained alkali feldspar granite, with the local development of medium- to coarse-grained alkali feldspar granite. It is primarily located in the central of Yizuomao Complex and mainly trend NE with long axis form. Lithology and mineral component for transient and rim phases are consistent with internal phase. The transient phase consists of medium- to fine-grained alkali feldspar granite and distributed as NE-trending. The rim phase is mainly composed of fine-grained alkali feldspar granite and distributed in the margin of Yizuomao Complex. The margins of the Yizuomao Complex were affected by tectonic activity, and the dykes are well developed in these areas. The majority of the dykes are granite porphyries (Fig. 2).

The stratigraphy of the Yizuomao region is dominated by Permian and Jurassic intermediate to silicis pyroclastic rock and siltstone. The Tumenling Formation is composed mainly of silty and argillaceous slate, siltstone, arkosic sandstone intercalated with marble. The Wudaoling Formation consists dominantly of rhyolite, rhyolite porphyry. Most of the mineral deposits around the Yizuomao Complex are hosted within the contact zone between the Tumenling or Wudaoling formations and granite porphyries (Fig. 2), including the Bailing Cu–Zn (Bo et al., 2016), the Wudaoling Mo–Fe (Shi et al., 2013), the Sujiaweizi Fe polymetallic (Li et al., 2015), and Erdaogou Pb–Zn deposits.

3. Samples and petrography

We collected the samples from the Yizuomao Complex, the Yizuomao Cu occurrence, the Wudaoling Mo–Fe deposit, the Bailing Cu–Zn and Sujiaweizi deposits, including biotite-bearing alkali-feldspar granite (samples YZM-1, YZM-1a, YZM-2, YZM-2a, YZM-3, YZM-3a, WDL-22, D-18, D-27, and D38), granite porphyry (CSC-1, BL-1, BL-2, BL-6, BL-7, BL-8, WDL-1, D32, and SJ-10). In the field, the Yizuomao Complex, granite porphyry is irregularly intruded into the Tumenling and Wudaoling formations along structural fracture, and strong skarnization occurred within contact zone between the granite porphyry, and Tumenling and Wudaoling formation. The sampling sites are shown in Figs. 1c and 2, and detailed petrographic descriptions of the rocks are given bellow.

3.1. Yizuomao Complex

The Yizuomao Complex is made up of medium- to coarse-grained (YZM-1, YZM-1a and D-27, Fig. 3a and b), medium- to fine-grained (YZM-2, YZM-2a, and D18, Fig. 3c and d), and fine-grained (YZM-3, YZM-3a and D38, Fig. 3e and f) biotite-bearing alkali feldspar granite. It contains K-feldspar (50–55%), quartz (35–40%), plagioclase (5–10%) and biotite (< 5%), along with accessory zircon and apatite. K-feldspar is subhedral to anhedral and some grains exhibit kaolinization and sericitization. Quartz crystals vary from euhedral to anhedral. Plagioclase is euhedral-subhedral and shows polysynthetic twinning.

3.2. Granite porphyry

The granite porphyry has a massive structure. The phenocrysts are mainly composed of K-feldspar (55–60%) with a grain size of 3–5 mm,

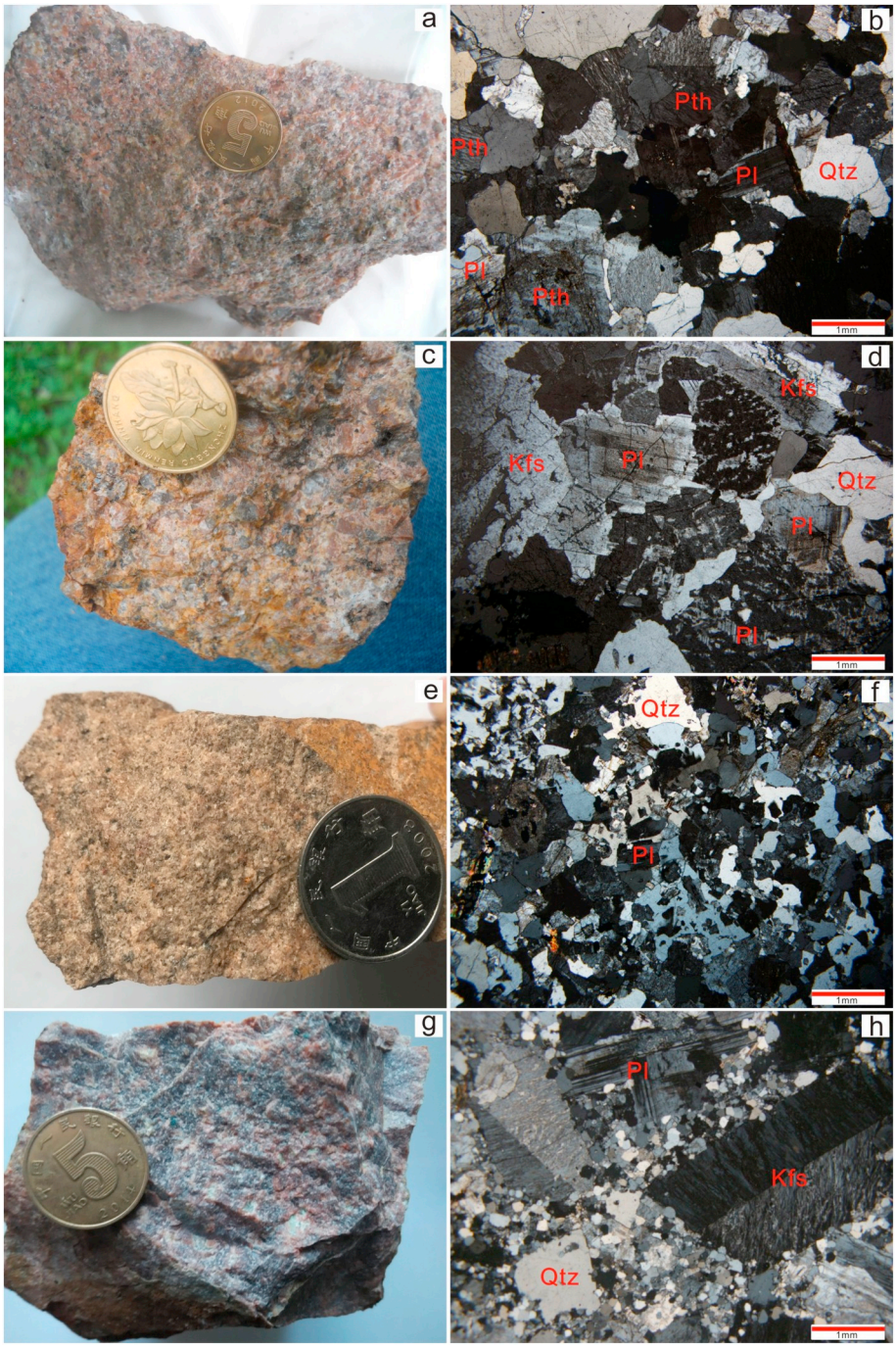

Fig. 3. Photographs and Photomicrographs of granitoids and mineralization–related rock in the Yizuomao area, showing (a) and (b) medium- to fine-grained biotite-bearing alkali-feldspar granite (Sample YZM-2); (c) and (d) medium- to coarse-grained biotite-bearing alkali-feldspar granite (Sample YZM-1); (e) and (f) fine-grained biotite-bearing alkali-feldspar granite (Sample YZM-3); (g) and (h) granite porphyry. Qtz = quartz; Pl = plagioclase, Pth = perthite; Kfs = K-feldspar.

Table 1
Major (wt%) and trace element (ppm) data for Early Jurassic intrusions in the Yizuomao area, eastern Ha'erbin.

Sample	D32	SJ-10[a]	WDL-1[b]	CSC-1[c]	BL-1[c]	BL-2[c]	BL-6[c]	BL-7[c]	BL-8[c]	YZM-1	YZM-1a	D18	YZM-2	YZM-2a	D27	YZM-3	YZM-3a	D38	WDL-22[b]
										Yizuomao Complex (alkali-feldspar granite)									
Rock	Granite porphyry									Medium- to coarse-grained			Medium- to fine-grained			Fine-grained			
SiO_2	63.94	74.58	75.86	76.16	65.19	63.89	65.67	70.27	66.25	76.60	76.75	76.54	75.03	74.56	73.33	76.32	76.92	73.57	75.81
Al_2O_3	18.51	12.57	12.51	12.70	14.10	14.42	14.81	13.72	15.27	12.64	12.62	12.41	13.06	13.58	14.57	12.44	12.23	14.21	12.79
TiO_2	0.49	0.16	0.14	0.10	0.50	0.59	0.42	0.44	0.49	0.15	0.12	0.13	0.23	0.21	0.19	0.18	0.13	0.09	0.15
Fe_2O_3	0.94	0.38	0.43	0.83	0.81	0.76	0.11	0.63	0.83	0.64	0.60	0.68	1.35	1.35	1.04	1.15	1.00	0.89	0.45
FeO	2.59	0.67	0.37	0.30	2.14	2.95	0.53	1.31	1.90	0.20	0.16	0.58	0.20	0.04	0.29	0.08	0.10	0.44	0.43
MnO	0.13	0.06	0.06	0.03	0.12	0.15	0.12	0.04	0.10	0.02	0.02	0.05	0.03	0.03	0.06	0.04	0.04	0.05	0.03
MgO	1.03	0.25	0.25	0.08	1.72	1.85	0.31	0.33	0.97	0.22	0.05	0.04	0.10	0.10	0.04	0.08	0.06	0.08	0.21
CaO	1.69	1.17	0.68	0.40	2.74	3.75	3.72	1.44	2.95	0.52	0.50	0.42	0.46	0.45	0.36	0.50	0.44	0.56	0.60
Na_2O	4.07	4.69	4.27	4.20	5.99	4.29	6.35	5.77	3.37	3.68	3.67	3.63	3.95	4.04	4.33	3.59	3.54	4.23	3.62
K_2O	4.09	4.56	4.57	4.48	3.58	3.41	4.62	4.13	4.21	4.72	4.76	4.97	4.56	4.59	4.96	4.71	4.74	5.09	4.90
P_2O_5	0.20	0.03	0.02	0.02	0.13	0.15	0.14	0.10	0.16	0.01	0.02	0.02	0.02	0.03	0.03	0.01	0.01	0.04	0.03
LOI	2.07	0.64	0.59	0.55	2.70	3.53	2.95	1.52	3.24	0.40	0.39	0.24	0.61	0.58	0.52	0.48	0.41	0.48	0.78
Total	99.76	99.75	99.73	99.85	99.72	99.75	99.76	99.70	99.75	99.80	99.81	99.70	99.78	99.78	99.73	99.79	99.76	99.72	99.80
TFe_2O_3	3.82	1.12	0.83	1.17	3.19	4.04	0.70	2.08	2.95	0.86	0.78	1.31	1.57	1.40	1.37	1.23	1.10	1.37	0.93
$Na_2O + K_2O$	8.17	9.25	8.84	8.68	9.57	7.70	10.98	9.90	7.58	8.40	8.44	8.60	8.51	8.64	9.29	8.30	8.28	9.32	8.51
Na_2O/K_2O	0.99	1.03	0.93	0.94	1.67	1.26	1.37	1.40	0.80	0.78	0.77	0.73	0.87	0.88	0.87	0.76	0.75	0.83	0.74
La	28.10	37.42	37.79	33.51	27.65	27.53	34.33	29.81	40.7	14.42	15.28	20.20	10.42	14.25	13.10	11.15	20.02	24.70	23.49
Ce	53.50	67.10	73.09	62.2	61.98	56.67	63.66	62.11	77.89	26.08	23.14	34.40	58.35	55.47	39.70	46.88	64.68	48.50	46.40
Pr	6.25	6.33	6.91	7.2	6.85	6.25	6.57	6.93	7.94	2.84	3.23	4.27	2.33	3.1	2.72	2.37	3.51	5.34	4.64
Nd	22.92	18.87	20.26	24.32	25.01	23.05	22.54	24.71	26.81	8.7	9.95	14.23	7.91	10.47	8.51	7.74	10.9	17.74	14.13
Sm	4.00	2.91	3.12	4.37	4.58	4.37	3.76	4.47	4.36	1.41	1.69	2.51	1.66	1.95	1.43	1.58	1.79	3.12	2.36
Eu	1.19	0.47	0.36	0.4	1.05	1.03	0.77	0.85	0.98	0.27	0.25	0.39	0.37	0.38	0.40	0.26	0.3	0.39	0.36
Gd	3.51	2.25	2.57	3.36	3.72	3.34	2.77	3.55	2.92	1.18	1.21	2.14	1.73	1.82	1.38	1.55	1.7	2.67	1.98
Tb	0.60	0.43	0.48	0.56	0.62	0.57	0.45	0.6	0.42	0.22	0.24	0.40	0.34	0.33	0.20	0.32	0.31	0.40	0.40
Dy	3.04	2.91	3.58	3.56	3.97	3.51	2.8	3.8	2.5	1.6	1.6	2.26	2.59	2.41	1.52	2.42	2.08	2.40	2.74
Ho	0.58	0.64	0.76	0.66	0.75	0.68	0.53	0.73	0.46	0.37	0.37	0.48	0.59	0.51	0.33	0.56	0.46	0.46	0.62
Er	1.81	2.18	2.82	2.03	2.31	2.13	1.69	2.30	1.36	1.45	1.43	1.62	2.09	1.78	1.10	1.98	1.62	1.42	2.24
Tm	0.30	0.42	0.49	0.34	0.35	0.32	0.25	0.35	0.20	0.33	0.32	0.32	0.42	0.36	0.22	0.41	0.32	0.23	0.42
Yb	2.05	3.20	3.74	2.25	2.51	2.25	1.84	2.47	1.33	2.74	2.68	2.33	3.28	2.71	1.69	3.20	2.48	1.62	3.16
Lu	0.30	0.50	0.60	0.34	0.39	0.35	0.29	0.40	0.22	0.43	0.43	0.37	0.53	0.45	0.26	0.50	0.41	0.25	0.53
Y	17.38	19.55	23.59	18.79	20.97	18.37	15.31	19.98	13.00	11.58	10.98	14.26	18.35	15.48	9.58	16.61	13.88	13.83	20.31
Rb	115.70	135.00	137.90	171.90	132.00	133.50	157.70	142.20	190.10	111.50	116.00	118.30	97.50	96.80	110.90	104.70	106.30	134.60	141.60
Sr	423.20	86.00	41.70	35.60	191.20	288.10	213.40	139.70	142.00	33.80	34.00	34.00	44.60	44.10	69.10	39.60	33.90	45.10	62.90
Zr	201.70	120.10	147.20	123.70	191.90	180.20	182.60	225.70	263.50	69.60	71.00	69.70	127.60	105.20	99.40	67.80	57.60	88.60	139.10
Nb	10.30	16.40	12.77	14.82	12.63	13.44	10.62	12.94	13.73	14.20	14.40	13.90	16.10	13.90	10.40	14.90	12.40	12.50	12.21
Ba	930.30	189.80	165.80	398.70	597.20	586.70	573.80	726.20	634.90	159.90	164.90	187.30	254.40	230.80	312.40	159.70	152.90	427.60	148.60
U	2.01	5.16	4.35	5.99	3.99	4.53	1.51	2.44	4.42	3.91	4.51	1.84	2.82	2.56	0.87	2.99	2.84	1.67	5.48
Th	7.85	15.36	15.18	18.81	11.79	12.57	7.37	9.25	14.29	17.72	20.72	17.69	16.81	16.14	8.24	17.42	18.08	11.68	22.61
Ta	0.95	1.49	1.17	1.45	1.17	1.22	0.82	1.12	1.11	2.33	2.42	1.58	2.18	2.08	0.93	2.13	2.06	0.99	1.13
Hf	5.40	4.46	6.15	4.82	5.85	5.82	5.10	6.75	5.93	3.14	3.14	3.00	5.39	4.50	3.60	2.78	2.51	3.30	5.66
LREE	115.96	133.10	141.54	132.00	127.12	118.90	131.63	128.88	158.68	53.72	53.54	76.00	81.04	85.62	65.86	69.98	101.20	99.79	91.37
HREE	12.19	12.54	15.05	13.10	14.62	13.15	10.62	14.20	9.41	8.32	8.28	9.92	11.57	10.37	6.70	10.94	9.38	9.45	12.08
ΣREE	128.15	145.64	156.59	145.10	141.74	132.05	142.25	143.08	168.09	62.04	61.82	85.92	92.61	95.99	72.56	80.92	110.58	109.24	103.45
δEu	0.95	0.54	0.38	0.31	0.75	0.79	0.70	0.63	0.79	0.62	0.51	0.50	0.66	0.61	0.86	0.50	0.52	0.40	0.50
$(La/Yb)_N$	9.24	7.88	6.81	10.04	7.43	8.25	12.58	8.14	20.63	3.55	3.84	5.84	2.14	3.55	5.23	2.35	5.44	10.28	5.01

Note: [a, b, c] Data from Li et al. (2012), Shi et al. (2012) and Bo et al. (2016), respectively.
LOI: Loss on ignition; δEu = (Eu)cn/[(Gd)cn + (Sm)cn]/2.
LREE = La + Ce + Pr + Nd + Sm + Eu; HREE = Gd + Tb + Dy + Ho + Er + Tm + Yb + Lu; ΣREE = LREE + HREE; $(La/Yb)_N$ = (La/0.310)/(Yb/0.209).

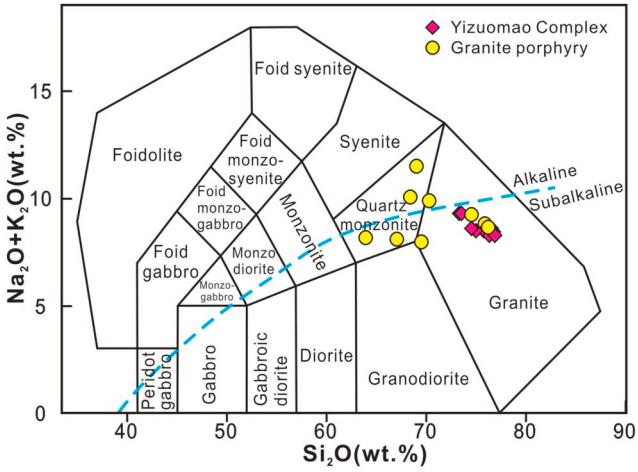

Fig. 4. SiO_2 vs. (Na_2O + K_2O) diagram (after Le Bas et al., 1986 and Le Maitre, 1989).

quartz (25–30%), and biotite (< 3%). The groundmass consists of quartz (55–65%), feldspar (30–35%), and minor biotite (< 5%), along with accessory zircon and apatite (Fig. 3h).

4. Analytical methods

4.1. Whole-rock geochemistry

The whole-rock major and trace element geochemical analysis was undertaken at the Key Laboratory of Applied Geochemistry, Chinese Academy of Geological Sciences. Samples were cleaned of altered surfaces and were crushed in an agate mill to a powder (~200 diameter mesh) at the Langfang Regional Geological Survey, Hebei Province, China. Major elements were determined by X-ray fluorescence (XRF) with analytical uncertainties ranging from 1% to 3%, and analytical precision is better than 5%. Trace element compositions were determined using an Agilent 7500a inductively coupled plasma mass spectrometer (ICP-MS), with detailed analytical procedures described in Gao et al. (2003).

4.2. Zircon U–Pb dating

Zircons were extracted from the biotite-bearing alkali-feldspar granite (YZM-1-1, YZM-2-1 and YZM-3-1) using standard density and magnetic separation techniques followed by handpicking using a binocular microscope at the Langfang Regional Geological Survey, Hebei Province, China. The handpicked zircons were examined using transmitted and reflected light, and their internal structures were imaged using employing a scanning electron microscope. The CL images were used to select domains within zircons for analysis. Zircon U–Pb ages were obtained using an Agilent 7500a ICP–MS equipped with a 193 nm laser at the State Key Laboratory of Geological Processes and Mineral Resources, China University of Geosciences, Wuhan, China. The 91500 zircon standard was used as an external standard for age calibration and a NIST SRM 610 silicate glass was used for instrument optimization during analysis. A 30 μm spot size was used during analysis and all other instrument parameters and procedures used are given in Yuan et al. (2004). The ICPMSDataCal (Ver. 6.7; Liu et al., 2008; Liu et al., 2010) and Isoplot (Ver. 3.0; Ludwig, 2003) programs were used for data reduction, and common Pb corrections were undertaken using the approach of Anderson (2002). The uncertainties on individual LA–ICP–MS analyses are quoted at the 1σ level, and errors on weighted mean ages are quoted at the 95% (2σ) confidence level.

4.3. Zircon Lu–Hf isotope

Zircon Hf isotope analysis was carried out in-situ using a ESI NWR193 laser-ablation microprobe, attached to a Neptune plus multi-collector ICP-MS at Beijing CreaTech Testing International Co., Ltd., Beijing. Instrumental conditions and data acquisition were comprehensively described by Wu et al. (2006) and Hou et al. (2007). A stationary spot was used for the present analyses, with a beam diameter of 40 μm depending on the size of ablated domains. Helium was used as carrier gas to transport the ablated sample from the laser-ablation cell to the ICP-MS torch via a mixing chamber mixed with Argon. In order to correct the isobaric interferences of ^{176}Lu and ^{176}Yb on ^{176}Hf, $^{176}Lu/^{175}Lu = 0.02658$ and $^{176}Yb/^{173}Yb = 0.796218$ ratios were determined (Chu et al., 2002). For instrumental mass bias correction Yb isotope ratios were normalized to $^{172}Yb/^{173}Yb$ of 1.35274 (Chu et al., 2002) and Hf isotope ratios to $^{179}Hf/^{177}Hf$ of 0.7325 using an exponential law. The mass bias behavior of Lu was assumed to follow that of Yb, mass bias correction protocols details was described as Wu et al. (2006) and Hou et al. (2007). Zircon GJ1was used as the reference standards during our routine analyses, with a weighted mean $^{176}Hf/^{177}Hf$ ratio of 0.282007 ± 0.000007 (2σ, n = 36). It is not distinguishable from a weighted mean $^{176}Hf/^{177}Hf$ ratio of 0.282000 ± 0.000005 (2σ) using a solution analysis method by Morel et al. (2008).

5. Results

5.1. Major and trace element geochemistry

The whole-rock major and trace element compositions of intrusions in the Yizuomao area are presented in Table 1. The data for the granitoids from the Yizuomao Complex all plot within the granite field (Fig. 4). These samples contain high concentrations of SiO_2 (73.33–76.92 wt%) and are enriched in alkalis (K_2O + Na_2O = 8.28–9.32 wt%; K_2O/Na_2O = 1.31–1.37), with K_2O and Na_2O concentrations of 3.62–4.33 wt% and 4.56–5.09 wt%, respectively. They contain low concentrations of TiO_2 (0.09–0.23 wt%), MnO (0.02–0.06 wt%), MgO (0.04–0.22 wt%), and CaO (0.36–0.56 wt%). The Yizuomao Complex has Al_2O_3 contents of 12.23 to 14.57 wt% and is peraluminous (Fig. 5a), with A/CNK [molar Al_2O_3/(CaO + Na_2O + K_2O)] values of 1.02–1.11. All samples belong to the high-K calc-alkaline series according to the K_2O vs. SiO_2 diagram (Fig. 5b).

Compared with the Yizuomao Complex, the granite porphyry within the quartz monzonite and granite fields (Fig. 4). The granite porphyries have SiO_2 contents of 63.89–76.16 wt% and are rich in alkalis (K_2O + Na_2O = 7.58–10.98 wt%; K_2O/Na_2O = 0.60–1.25), with K_2O and Na_2O concentrations of 3.58–4.62 and 3.37–5.99 wt%, respectively. Data for most samples plot within the metaluminous and peralkaline fields in an A/CNK vs. A/NK diagram, except two samples that lie within the peraluminous field (Fig. 5a). All samples belong to the high–K calc–alkaline series on a SiO_2 vs. K_2O diagram (Fig. 5b).

Chondrite-normalized rare earth element (REE) patterns (Fig. 6a) of rocks from the Yizuomao Complex are characterized by a strong enrichment in light REE relative to heavy REE with $(La/Yb)_N$ ratios of 18.95 to 23.95, and clear negative Eu anomalies (δEu = 0.50–0.66, mean = 0.57) and positive Ce anomalies. On a primitive-mantle-normalized trace element diagram (Fig. 6b), rocks of the complex are characterized by enrichment in Rb, Th, U, K, and Pb, and depletion in Ba, Nb, Sr and Ti, and have distinct negative Sr and Ba anomalies that are consistent with the fractionation of feldspar.

REE patterns (Fig. 6a) for the rocks from granite porphyry exhibit a strong enrichment in LREEs with $(La/Yb)_N$ ratios of 8.95 to 17.95 and variably negative Eu anomalies (δEu = 0.31–0.95, mean = 0.65). On a primitive-mantle-normalized trace element diagram (Fig. 6b), the granite porphyries show strong enrichment in large-iron lithophile

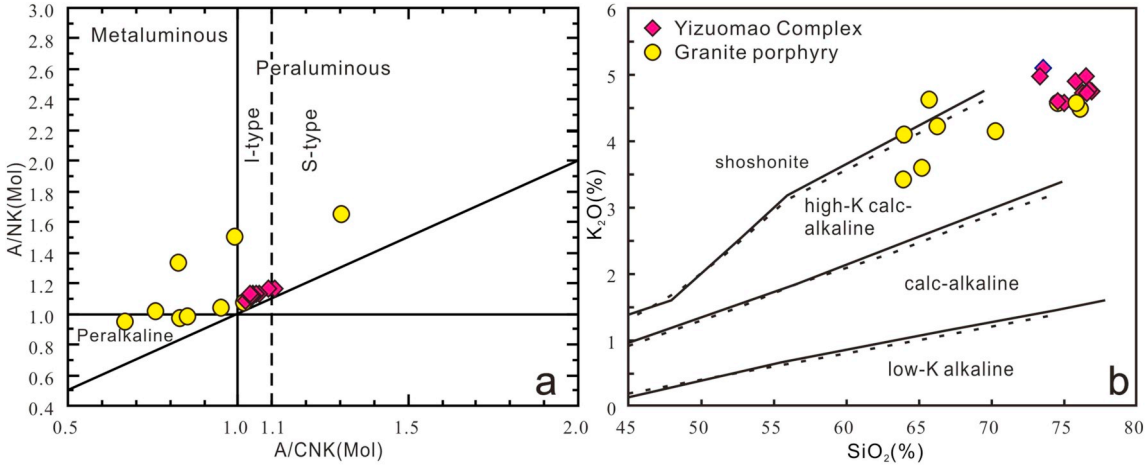

Fig. 5. A/KNC vs. A/NK diagram, where A/KNC = Al_2O_3 (molar)/(K_2O + Na_2O + CaO) (molar), A/NK = Al_2O_3 (molar)/(Na_2O + K_2O) (after Frost et al., 2001); (d) SiO_2 vs. K_2O diagram (after Whalen et al., 1987).

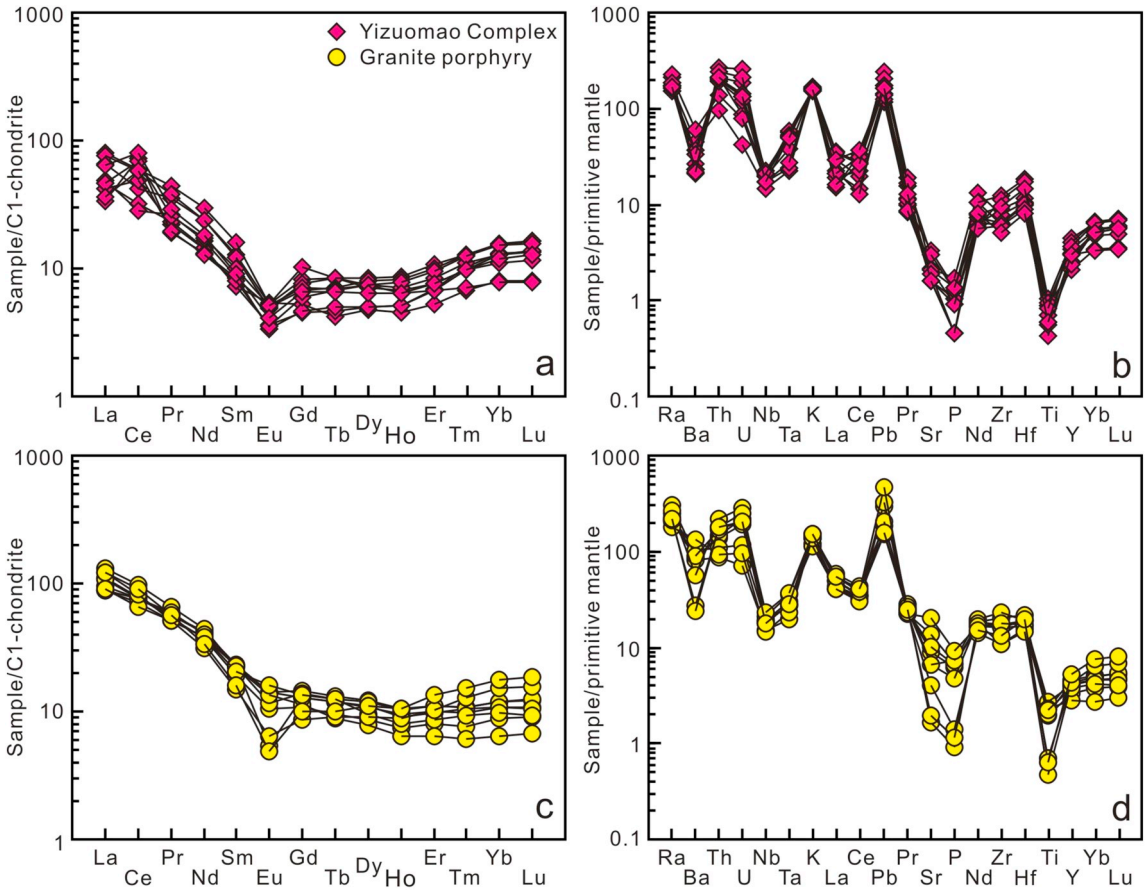

Fig. 6. Chondritenormalized REE patterns (a and c) and primitive mantle-normalized trace element spidergrams (b and d). Chondrite and primitive mantle values taken from Boynton (1984) and Sun and McDonough (1989), respectively.

elements (LILEs; e.g., Rb, Th, U, K and Pb) relative to high-field-strength elements (HFSEs) and light REEs, as well as significant depletion in Nb, Ta, P, and Ti, which is consistent with the geochemical characteristics of subduction-related magmas.

5.2. U–Pb zircon geochronology

Sample YZM-1 is a medium- to fine-grained, biotite-bearing, alkali-feldspar granite from the Yizuomao Complex (45°21′23.4″N, 127°13′11.7″E; Fig. 2a). Zircon crystals are typically euhedral to subhedral, with lengths of 50 to 150 μm. The zircons contain 750–1441 ppm (ppm) U and 438–1214 ppm Th. Th/U ratios range from 0.52 to 0.93 (Table 2), indicating that the zircons are of igneous origin (Belousova et al., 2002), consistent with the oscillatory zoning and prismatic grain shapes (Fig. 7). A total of 16 analytical spots yield a $^{206}Pb/^{238}U$ mean age of 195.3 ± 1.8 Ma (MSWD = 0.54, n = 11; Fig. 8a and b), interpreted to represent the crystallization age of the biotite-bearing alkali feldspar granite. Several zircons with older age of 218–199 Ma (Table 2) are interpreted as inherited grains entrained by the magma.

Table 2
LA-ICP-MS zircon U–Pb dating data of the Yizuomao Complex.

Sample no.	Th (ppm)	U (ppm)	Th/U	Isotopic ratios						Ages (Ma)					
				$^{207}Pb/^{206}Pb$		$^{207}Pb/^{235}U$		$^{206}Pb/^{238}U$		$^{207}Pb/^{206}Pb$		$^{207}Pb/^{235}U$		$^{206}Pb/^{238}U$	
				Ratio	1σ	Ratio	1σ	Ratio	1σ	Age	1σ	Age	1σ	Age	1σ
YZM-1-01	836	1441	0.58	0.05032	0.00248	0.21321	0.01067	0.03063	0.00047	210	88	196	9	191	3
YZM-1-02	642	1226	0.52	0.05434	0.00433	0.22906	0.01791	0.03057	0.00047	385	183	209	15	193	3
YZM-1-03	726	1094	0.66	0.05603	0.00352	0.23469	0.01406	0.03082	0.00053	454	103	214	12	194	3
YZM-1-04	636	918	0.69	0.0491	0.00282	0.21052	0.01145	0.03128	0.00048	153	96	194	10	194	3
YZM-1-05	829	1207	0.69	0.05407	0.00479	0.24382	0.02128	0.0327	0.0005	374	203	222	17	194	3
YZM-1-06	697	1084	0.64	0.05032	0.00327	0.23351	0.01542	0.03342	0.00055	210	120	213	13	196	3
YZM-1-07	438	750	0.58	0.0508	0.00393	0.22403	0.01698	0.03225	0.00075	232	130	205	14	196	5
YZM-1-08	698	1052	0.66	0.05216	0.00308	0.21675	0.01224	0.03032	0.00057	292	94	199	10	196	4
YZM-1-10	442	790	0.56	0.05406	0.00513	0.25276	0.02153	0.03439	0.0007	374	156	229	17	196	4
YZM-1-11	694	1043	0.67	0.0499	0.00377	0.21139	0.01575	0.03049	0.0006	190	132	195	13	198	4
YZM-1-13	634	933	0.68	0.04758	0.00249	0.20684	0.01092	0.03114	0.00042	78	92	191	9	199	3
YZM-1-14	953	1320	0.72	0.04955	0.00245	0.21437	0.01066	0.03091	0.00043	174	89	197	9	205	3
YZM-1-15	762	1059	0.72	0.05079	0.00349	0.2185	0.01491	0.03093	0.00052	232	125	201	12	205	3
YZM-1-18	782	1245	0.63	0.05117	0.00287	0.21306	0.01123	0.03003	0.00043	249	95	196	9	207	3
YZM-1-19	1214	1295	0.94	0.04989	0.00522	0.22209	0.0228	0.03228	0.00066	190	235	204	19	212	4
YZM-1-20	674	1035	0.65	0.05816	0.00409	0.24586	0.01606	0.03087	0.00054	536	112	223	13	218	3
YZM-2-01	465	635	0.73	0.057	0.00468	0.24879	0.02046	0.0317	0.00059	491	150	226	17	201	4
YZM-2-02	552	849	0.65	0.05297	0.00479	0.2367	0.02092	0.03245	0.00062	327	166	216	17	206	4
YZM-2-03	458	728	0.63	0.05283	0.0051	0.23588	0.02232	0.03263	0.00071	321	174	215	18	207	4
YZM-2-04	496	759	0.65	0.05047	0.00536	0.25365	0.02914	0.03563	0.00087	217	213	230	24	226	5
YZM-2-05	507	741	0.68	0.05201	0.00533	0.25271	0.02458	0.0356	0.00078	286	180	229	20	225	5
YZM-2-06	770	1067	0.72	0.0521	0.00498	0.22041	0.02074	0.03068	0.0005	290	219	202	17	195	3
YZM-2-07	930	1410	0.66	0.05179	0.00309	0.23484	0.01453	0.0328	0.00052	276	113	214	12	208	3
YZM-2-08	1006	1165	0.86	0.0553	0.0041	0.24861	0.01793	0.03261	0.00061	425	128	225	15	207	4
YZM-2-09	419	537	0.78	0.05273	0.0046	0.22812	0.02032	0.03083	0.00077	317	156	209	17	196	5
YZM-2-10	552	730	0.76	0.05541	0.0037	0.23338	0.0156	0.0306	0.00059	429	115	213	13	194	4
YZM-2-11	757	1277	0.59	0.05602	0.00315	0.2613	0.01522	0.03369	0.0006	453	97	236	12	214	4
YZM-2-12	877	908	0.97	0.05538	0.00342	0.23614	0.01364	0.03164	0.0005	428	101	215	11	201	3
YZM-2-13	424	617	0.69	0.05059	0.00418	0.20885	0.0173	0.02999	0.00071	222	144	193	15	190	4
YZM-2-14	810	1232	0.66	0.04983	0.00247	0.22139	0.0109	0.03232	0.0005	187	85	203	9	205	3
YZM-2-15	811	935	0.87	0.05349	0.00395	0.23119	0.01716	0.03111	0.00058	350	135	211	14	197	4
YZM-2-16	517	904	0.57	0.04778	0.00287	0.20731	0.01244	0.03126	0.00046	88	106	191	10	198	3
YZM-2-17	833	621	1.34	0.05427	0.00412	0.24434	0.01788	0.03287	0.00056	382	135	222	15	208	3
YZM-2-18	1008	1208	0.83	0.0517	0.00324	0.2258	0.0146	0.03154	0.00053	272	118	207	12	200	3
YZM-2-19	536	742	0.72	0.05165	0.00345	0.22509	0.01477	0.03199	0.00054	270	120	206	12	203	3
YZM-2-20	602	650	0.93	0.05104	0.00385	0.20907	0.01608	0.0297	0.00052	243	143	193	14	189	3
YZM-3-01	559	814	0.69	0.05532	0.00462	0.25214	0.02068	0.03409	0.00069	425	148	228	17	216	4
YZM-3-02	582	895	0.65	0.04609	0.00589	0.21688	0.02726	0.03413	0.00077	2	242	199	23	216	5
YZM-3-03	770	1086	0.71	0.05069	0.00478	0.21987	0.02037	0.03146	0.00057	227	215	202	17	200	4
YZM-3-04	365	594	0.61	0.04889	0.00432	0.22746	0.01961	0.03374	0.00064	143	200	208	16	214	4
YZM-3-05	453	725	0.62	0.05203	0.0044	0.23288	0.02073	0.03243	0.00067	287	164	213	17	206	4
YZM-3-06	797	1035	0.77	0.05943	0.00415	0.25155	0.01635	0.03106	0.00047	583	115	228	13	197	3
YZM-3-07	2281	2223	1.03	0.06627	0.0063	0.29159	0.02712	0.03191	0.00062	815	206	260	21	203	4
YZM-3-08	1197	1264	0.95	0.05446	0.00425	0.22613	0.01684	0.03066	0.00086	390	117	207	14	195	5
YZM-3-09	562	834	0.67	0.05626	0.00509	0.249	0.02268	0.03239	0.00079	463	160	226	18	206	5
YZM-3-10	581	1502	0.39	0.05181	0.00407	0.2379	0.01824	0.0333	0.00057	277	180	217	15	211	4
YZM-3-13	1115	1522	0.73	0.05261	0.00252	0.24213	0.01129	0.03341	0.00047	312	80	220	9	212	3
YZM-3-14	1378	2029	0.68	0.05567	0.0045	0.23972	0.01896	0.03123	0.00051	439	185	218	16	198	3
YZM-3-15	739	980	0.75	0.05003	0.00372	0.22805	0.01685	0.03288	0.00063	197	132	209	14	209	4
YZM-3-16	547	1207	0.45	0.05434	0.0043	0.25263	0.02007	0.03398	0.00067	385	144	229	16	215	4
YZM-3-18	628	947	0.66	0.06053	0.00788	0.25396	0.03277	0.03043	0.00051	622	294	230	27	193	3
YZM-3-19	1264	1343	0.94	0.05229	0.0045	0.24218	0.02089	0.03369	0.00065	298	160	220	17	214	4
YZM-3-20	453	736	0.62	0.05398	0.0069	0.23526	0.02969	0.03161	0.00066	370	289	215	24	201	4

Sample YZM-2 is a medium-grained, biotite-bearing, alkali feldspar granite from the Yizuomao Complex (45°19′05.4″N, 127°15′38.3″E; Fig. 2c). Zircon crystals are typically euhedral to subhedral, with lengths of 60 to 200 μm. The zircons contain 537–1410 ppm U and 419–1008 ppm Th. Th/U ratios range from 0.57 to 1.34 (Table 2), suggesting that the zircons are of igneous origin (Belousova et al., 2002), consistent with the oscillatory zoning and prismatic grain shapes (Fig. 7). Eighteen analytical spots yield a $^{206}Pb/^{238}U$ mean age of 200.6 ± 3.2 Ma (MSWD = 0.94, n = 18; Fig. 8c and d), which is interpreted as the crystallization age of the biotite-bearing alkali feldspar granite. The remaining two spots yielded ages of 226 and 225 Ma (Table 2), interpreted to be inherited zircons entrained by the magma.

Sample YZM-3 is a medium- to fine-grained, biotite-bearing, alkali feldspar granite from the Yizuomao Complex (45°19′04.5″N, 127°15′38.3″E; Fig. 2e). Zircon crystals are typically euhedral to subhedral, with lengths of 30 to 130 μm. The zircons contain 594–2223 ppm U and 365–2281 ppm Th. Th/U ratios range from 0.39 to 1.03 (Table 2), indicating that the zircons are of igneous origin (Belousova et al., 2002), which is consistent with the oscillatory zoning and prismatic grain shapes (Fig. 7). Seventeen analytical spots yielded a $^{206}Pb/^{238}U$ mean age of 205.2 ± 4.1 Ma (MSWD = 4.6, n = 17; Fig. 8e and f), which is interpreted as the crystallization age of the biotite-bearing alkali feldspar granite.

Samples CSC-1 and BL-1 were collected from the surface and drilling hole No. ZK18 in the Bailing Cu–Zn deposit, respectively. Our research team had obtained the zircon U–Pb ages from these samples and

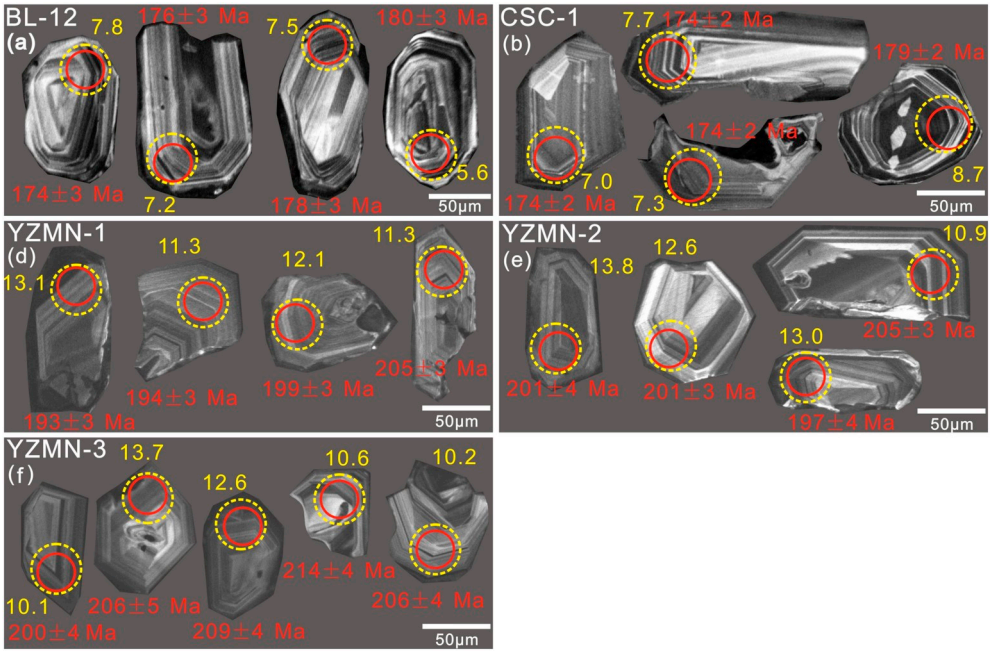

Fig. 7. Representative Cathodoluminescence (CL) images of zircons from intrusions with analytical numbers, U–Pb ages, $\varepsilon_{Hf}(t)$ values. The analyzed spots of the zircon U–Pb age and in-situ Hf isotope are represented by the red and yellow circles, respectively. (For interpretation of the references to color in this figure legend, the reader is referred to the web version of this article.)

published the results (Bo et al., 2016; Shi et al., 2012). Sample CSC-1 yielded $^{206}Pb/^{238}U$ mean age of 175.6 ± 1.3 Ma (MSWD = 1.9, n = 19; Bo et al., 2016), and sample BL-12 yielded $^{206}Pb/^{238}U$ mean ages of 189.0 ± 2.6 Ma (MSWD = 0.72, n = 5) and 178.2 ± 1.5 Ma (MSWD = 1.11, n = 15; Bo et al., 2016). The ages of 175.6 ± 1.3 Ma and 178.2 ± 1.5 Ma are interpreted as representing the crystallization age of samples CSC-1 and BL-1.

5.3. Zircon Hf isotopes

In situ zircon Hf isotope analysis for samples CSC-1 and BL-1 were from corresponding age dating samples, which were measured zircon U–Pb ages by our research team previously. The results of in situ Hf isotopic analyses results are given in Table 3 and plotted in Fig. 9. The $f_{Lu/Hf}$ values for all samples varying from −0.97 to −0.87, significantly lower than those values of the mafic crust ($f_{Lu/Hf}$ = −0.34, Amelin et al., 1999) and silicic crust ($f_{Lu/Hf}$ = −0.72, Vervoort and Jonathan Patchett, 1996). These data permit calculation of two-stage model ages that constrain the time of the extraction of the source material from the depleted mantle or the residence time of the source material in the crust (Blichert-Toft and Albarède, 1997).

A total 24 spots analyzed for zircons from the Yizuomao Complex show positive $\varepsilon_{Hf}(t)$ values that vary from +8.5 to +14.3, and cluster within the range of +10 to +13 (Fig. 9, Table 3). These positive $\varepsilon_{Hf}(t)$ values indicate a predominant contribution of juvenile crust to the granitoid sources. Initial $^{176}Hf/^{177}Hf$ ratios range from 0.282902 to 0.283060, corresponding to the depleted mantle two-stage Hf model ages (T_{DM2}) of 327–686 Ma (Table 3). Twenty spots analyzed for zircons from the granite porphyries show positive $\varepsilon_{Hf}(t)$ values of +5.6 to +11.6 and cluster within the range of +6 to +9 (Fig. 9, Table 3). Their initial $^{176}Hf/^{177}Hf$ ratios range from 0.282823 to 0.282990, corresponding to the depleted mantle two-stage Hf model ages (T_{DM2}) of 492–864 Ma (Table 3). In a $\varepsilon_{Hf}(t)$ vs. U–Pb age diagram, all the zircon Lu–Hf isotopic data plot in the field for the eastern CAOB proposed by Xiao et al. (2004) and Chen et al. (2009), but outside of the field defined by zircons from the Yanshan Fold and Thrust Belt proposed by Yang et al. (2006; Fig. 9a).

6. Discussion

6.1. Timing of magmatism and mineralization

Zircon U–Pb ages of the biotite-bearing alkali feldspar granite are 195.3 ± 1.8 Ma, 200.6 ± 3.2 Ma and 205.2 ± 4.1 Ma, indicating that the Yizuomao Complex was emplaced during the Late Triassic to Early Jurassic. The emplacement ages of the granite porphyries are 175.6 ± 1.3 Ma and 178.2 ± 1.5 Ma. Field observations, the ages of the Yizuomao Complex and granite porphyries, as well as skarn mineralization indicate that metallogenesis occurred around the margins of the Yizuomao Complex, and that granite porphyries emplaced into the Yizuomao Complex are spatially associated with skarn mineralization at their contacts. However, no skarns have been observed at the contact between the Yizuomao Complex and carbonate strata. Therefore, we consider that the granite porphyries around the Yizuomao Complex are closely associated with the presence of skarns. The geological characteristics of the deposits, combined with the zircon U–Pb ages for the granite porphyries associated with the Yizuomao Cu occurrence, Bailing Cu–Zn, and Wudaoling Mo deposits, indicate that mineralization in the Yizuomao area was genetically related to granite porphyries emplacement.

Magmatism in the Zhangguangcai Range occurred during the Late Triassic–Middle Jurassic (175–222 Ma, Wu et al., 2011a, 2011b). The Mo mineralization occurred in three main stage [Early Triassic (248–242 Ma), Jurassic (178–146 Ma), and Early Cretaceous (142–131 Ma)] in the East Xingmeng orogenic belt, northeast China (Zeng et al., 2012), or two stages [195–165 Ma and 115–110 Ma (Sun et al., 2012a, 2012b), as well as the Early Yanshanian] in the Lesser Xing'an Range-Zhangguangcai mountains (Yang et al., 2012). A number of deposits have been discovered in the northeast of Heilongjiang-Jilin area, including Mo deposits (e.g. Dashihe, Fu'anpu, Sancha and Dongfeng), Cu polymetallic deposits (e.g. Yanghuidongzi and Jiufogou). The timing of these deposits is consistent with an episode of Mo mineralization at 190–160 or 195–165 Ma. This observation, together with the abundance of Mo and Cu polymetallic deposits in eastern Jilin and Heilongjiang provinces, suggests that a significant Fe, Pb, Zn, Mo, and Cu polymetallic mineralization event occurred between the Early and Middle Jurassic in the Yizuomao area (Table 4).

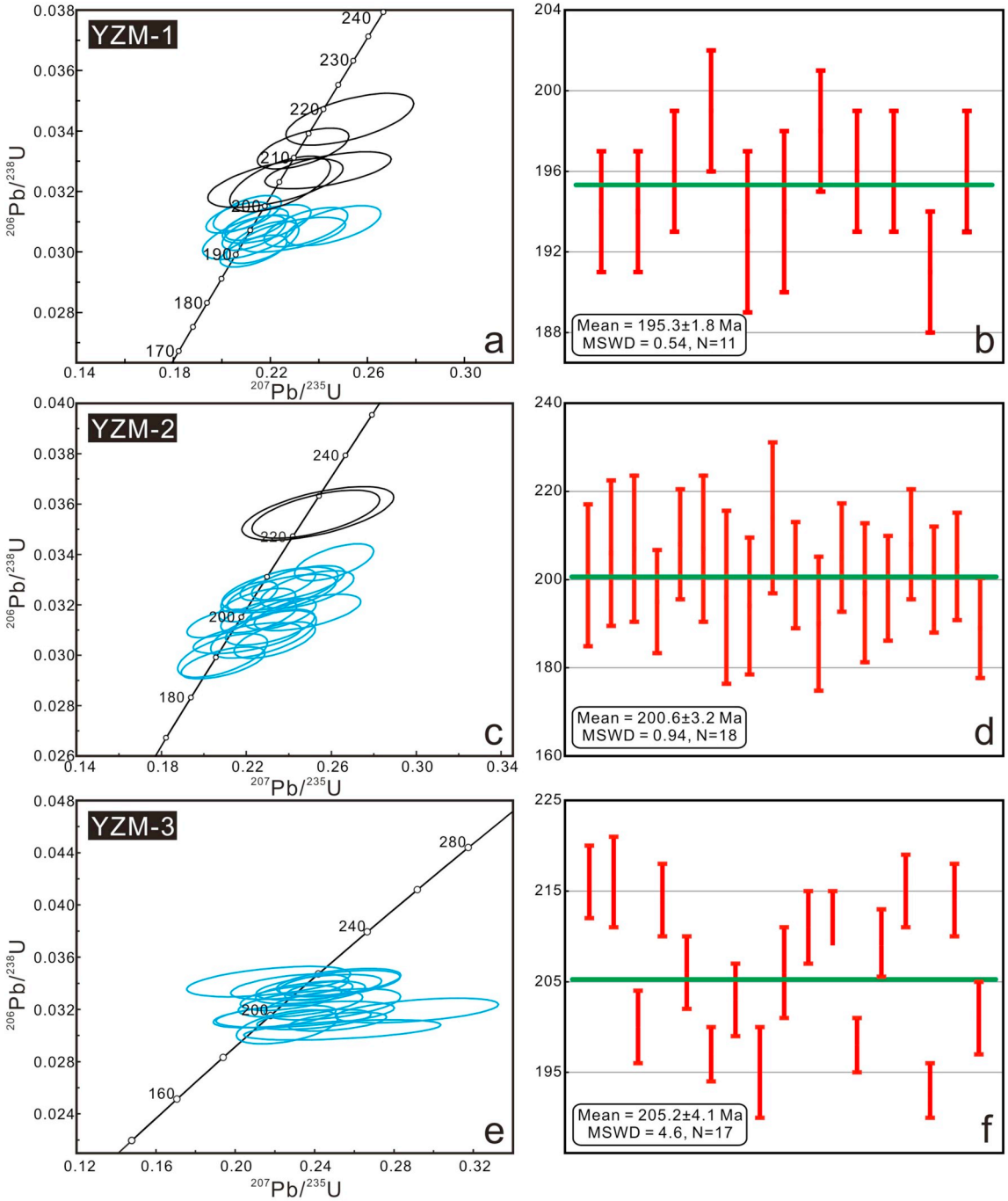

Fig. 8. Zircon LA–ICP–MS dating results for the biotite-bearing alkali-feldspar granite samples YZM-1, YZM-2 and YZM-3. (a), (c) and (e): concordant ages; (b), (d) and (f): weighted mean ages.

6.2. Magma source and petrogenesis

Many studies have examined highly fractionated I-type granites in China (e.g., Li et al., 2007a, 2007b; Wu et al., 2003a, 2003b). The Yizuomao Complex and associated granite porphyry contain high concentrations of SiO_2 and $K_2O + Na_2O$, and low concentrations of Ti, Fe, Mn, and Ca. They are also generally depleted in Ba, Nb, Sr, and Ti, and enriched in Rb, Th, U, K and Pb, with high Rb/Sr ratios, indicating that the magmas that formed the granitoids were highly fractionated (Chappell, 1999; Wu et al., 2003a). Furthermore, data for the majority of the samples analyzed during this study plot within the fields for highly fractionated granite in $(K_2O + Na_2O)/CaO$ and $10{,}000 * Ga/Al$ vs. (Zr + Nb + Ce + Y) discrimination diagrams (Fig. 10a and b). The Yizuomao Complex and most of the granite porphyries are weakly peraluminous (A/CNK < 1.1; A/NK > 1.0), thus differing from S-type granites, which are typically strongly peraluminous (A/CNK > 1.1; Chappell and White, 1974; Clemens, 2003; Wu et al., 2007b). The very low concentrations of P_2O_5 (≤ 0.10 wt%) are negatively correlated with SiO_2, and Th correlates positively with Rb, which are consistent with the fractionation trends of I-type magmas (Fig. 11a and b; Chappell, 1999; Li et al., 2007a, 2007b; Wu et al., 2003a, 2003b). Thus, we conclude that the Yizuomao Complex and associated granite porphyries represent highly fractionated I-type granites, similar to the Xinhuatun pluton, which is located ca. 45 km to the northeast of the present study area (Wu et al., 2003a).

Previous studies have suggested that the highly fractionated I-type

Table 3
Zircon Lu–Hf isotopic data for Early Jurassic intrusions in the Yizuomao area, eastern Ha'erbin.

Spot number	Age (Ma)	$^{176}Yb/^{177}Hf$	$^{176}Lu/^{177}Hf$	$^{176}Hf/^{177}Hf$	2σ	ε_{Hf} (0)	ε_{Hf} (t)	T_{DM1} (Ma)	T_{DM2} (Ma)	$f_{Lu/Hf}$
YZM-3-3	200	0.061852	0.001994	0.282940	0.000030	6.0	10.1	454	594	−0.94
YZM-3-5	206	0.042719	0.001390	0.282939	0.000027	5.9	10.2	448	588	−0.96
YZM-3-7	203	0.087157	0.002777	0.283060	0.000031	10.2	14.3	285	327	−0.92
YZM-3-8	195	0.066821	0.002155	0.282974	0.000026	7.1	11.1	407	522	−0.94
YZM-3-9	206	0.045023	0.001491	0.283038	0.000025	9.4	13.7	307	366	−0.96
YZM-3-15	209	0.053020	0.001752	0.283005	0.000028	8.2	12.6	357	441	−0.95
YZM-3-16	215	0.042889	0.001699	0.282970	0.000023	7.0	11.5	407	515	−0.95
YZM-3-19	214	0.068846	0.002655	0.282948	0.000039	6.2	10.6	450	575	−0.92
YZM-1-2	193	0.067518	0.002371	0.283032	0.000033	9.2	13.1	323	393	−0.93
YZM-1-4	194	0.046036	0.001592	0.282977	0.000023	7.2	11.3	396	512	−0.95
YZM-1-13	199	0.046205	0.001709	0.282996	0.000025	7.9	12.1	370	466	−0.95
YZM-1-14	205	0.047442	0.001790	0.282972	0.000029	7.1	11.3	406	518	−0.95
YZM-1-15	205	0.054553	0.002098	0.283039	0.000028	9.4	13.7	311	369	−0.94
YZM-1-18	207	0.044199	0.001538	0.282996	0.000025	7.9	12.2	368	461	−0.95
YZM-1-20	218	0.063912	0.002230	0.283002	0.000022	8.1	12.6	367	447	−0.93
YZM-2-1	201	0.075566	0.002808	0.283048	0.000031	9.7	13.8	304	357	−0.92
YZM-2-9	196	0.077783	0.002650	0.282987	0.000029	7.6	11.6	393	496	−0.92
YZM-2-12	201	0.048123	0.001615	0.283010	0.000025	8.4	12.6	348	432	−0.95
YZM-2-13	190	0.050418	0.001975	0.282902	0.000039	4.6	8.5	509	686	−0.94
YZM-2-14	205	0.052431	0.001798	0.282960	0.000024	6.6	10.9	423	546	−0.95
YZM-2-15	197	0.074368	0.002576	0.283027	0.000033	9.0	13.0	332	403	−0.92
YZM-2-16	198	0.041539	0.001491	0.283017	0.000024	8.7	12.8	337	417	−0.96
YZM-2-18	200	0.055323	0.001974	0.283024	0.000026	8.9	13.1	331	404	−0.94
YZM-2-19	203	0.045811	0.001650	0.282934	0.000023	5.7	10.0	459	604	−0.95
CSC-1-1	179	0.039452	0.001293	0.282910	0.000024	4.9	8.7	488	668	−0.96
CSC-1-2	176	0.052134	0.001732	0.282919	0.000023	5.2	8.9	481	654	−0.95
CSC-1-7	175	0.026325	0.000882	0.282886	0.000027	4.0	7.8	517	723	−0.97
CSC-1-8	176	0.059715	0.001897	0.282928	0.000027	5.5	9.2	471	635	−0.94
CSC-1-9	177	0.047153	0.001584	0.282955	0.000026	6.5	10.2	428	571	−0.95
CSC-1-10	174	0.045105	0.001437	0.282887	0.000026	4.1	7.7	523	724	−0.96
CSC-1-11	176	0.031913	0.001061	0.282894	0.000029	4.3	8.1	508	704	−0.97
CSC-1-12	175	0.062471	0.001998	0.282963	0.000030	6.8	10.4	420	556	−0.94
CSC-1-16	174	0.035581	0.001172	0.282865	0.000030	3.3	7.0	551	772	−0.96
CSC-1-20	174	0.034889	0.001137	0.282873	0.000024	3.6	7.3	539	755	−0.97
BL-12-1	176	0.033495	0.001205	0.282870	0.000025	3.5	7.2	544	760	−0.96
BL-12-2	174	0.031503	0.001100	0.282888	0.000022	4.1	7.8	518	721	−0.97
BL-12-3	181	0.037631	0.001307	0.282889	0.000021	4.2	8.0	518	715	−0.96
BL-12-4	178	0.027422	0.000991	0.282876	0.000026	3.7	7.5	533	744	−0.97
BL-12-6	179	0.040858	0.001522	0.282864	0.000023	3.2	7.0	558	775	−0.95
BL-12-8	179	0.037323	0.001276	0.282858	0.000026	3.0	6.8	563	787	−0.96
BL-12-10	180	0.031490	0.001309	0.282851	0.000032	2.8	6.6	573	802	−0.96
BL-12-11	179	0.026809	0.000976	0.282896	0.000025	4.4	8.2	504	698	−0.97
BL-12-16	178	0.030374	0.001118	0.282845	0.000026	2.6	6.4	578	815	−0.97
BL-12-17	180	0.038148	0.001271	0.282823	0.000025	1.8	5.6	612	864	−0.96

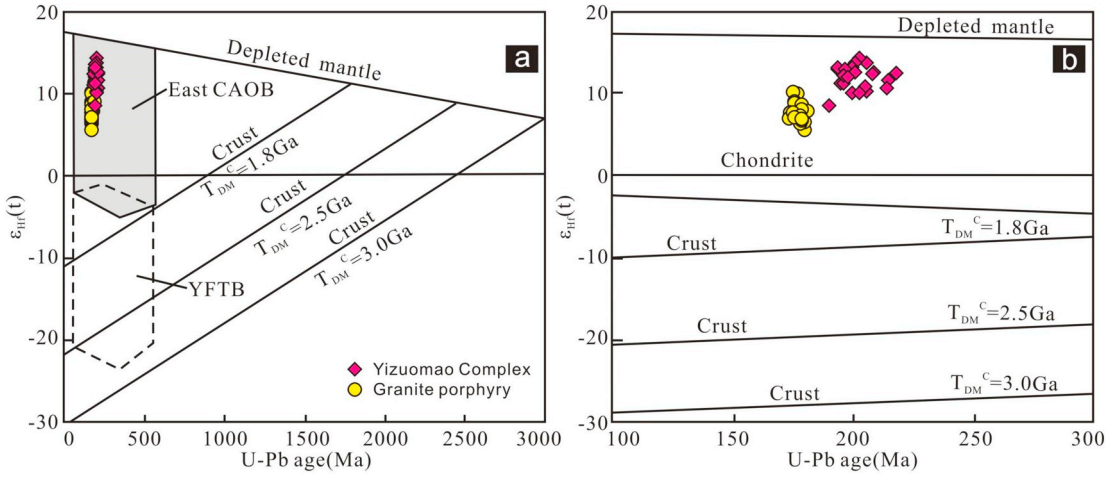

Fig. 9. Zircon $\varepsilon_{Hf}(t)$ values vs. U–Pb ages of zircons.

granites are produced by: (a) partial melting of crustal material (Chappell, 1999; Barbarin, 1996; Chappell et al., 2012), or (b) the final stage of fractional crystallization of mafic melts (Cawthorn and Brown, 1976; Chappell, 1999; Wyborn et al., 2001). The Yizuomao Complex and granite porphyries are characterized by a narrow range of compositions, and mafic rocks in the area are rare. Thus, it is unlikely that these granitoids were produced by fractional crystallization. The Yizuomao Complex granites and granite porphyries also have low Nb/Ta

Table 4
Ages of granitoids and mineralization–related rock from our research team in the Yizuomao area.

Deposit/Pluton	Lithology	Measured objects	Method	Age (Ma)	Reference
Yizuomao Cu occurrence	Granite porphyry	Zircon	LA–ICP–MS U–Pb	175.6 ± 1.3 (n = 19) 196 ± 3 (n = 1)	Bo et al., 2016
Bailing Cu–Zn deposit				177.7 ± 1.5 (n = 15) 189.0 ± 2.6 (n = 5)	
Yizuomao Complex	Medium- to fine-grained biotite-bearing alkali-feldspar granite Medium-grained biotite-bearing alkali-feldspar granite Medium- to fine-grained biotite-bearing alkali-feldspar granite			195.3 ± 1.8 Ma (n = 11) 200.6 ± 3.2 Ma (n = 18) 205.2 ± 4.1 Ma (n = 17)	This study

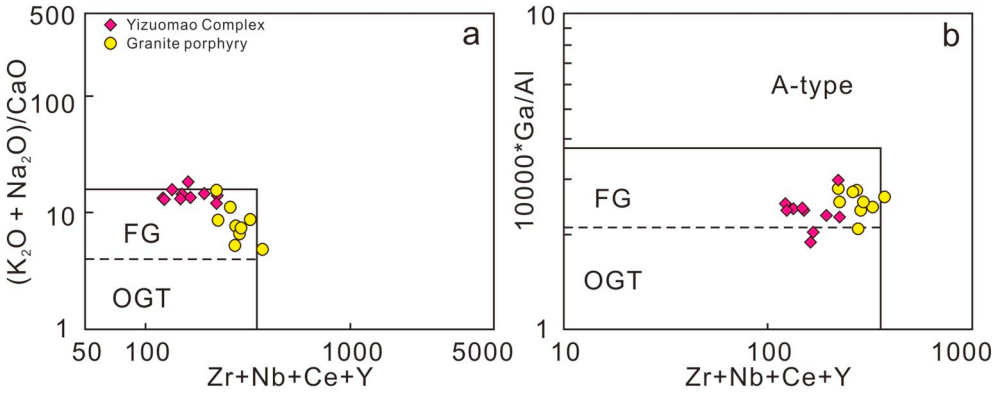

Fig. 10. ($K_2O + Na_2O$)/CaO vs. Zr + Nb + Ce + Y (a) and 1000 * Ga/Al vs. Zr + Nb + Ce + Y diagrams (b). Both diagrams are modified from Whalen et al., 1987. FG = fractionated M-, I-, and S-type granites; OGT = unfractionated M-, I-, and S-type granites.

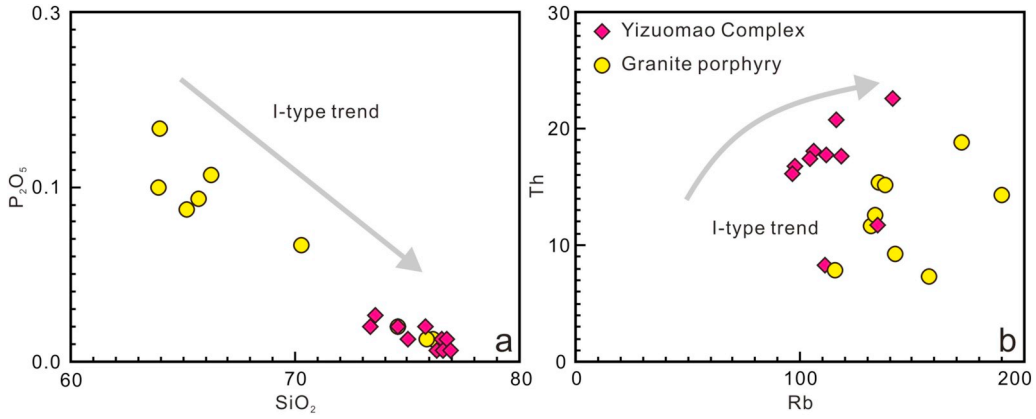

Fig. 11. P_2O_5 vs. SiO_2 (a) and Th vs. Rb (b) diagrams. Field of East CAOB and YFTB are from Xiao et al., 2004; Chen et al., 2009; Yang et al., 2006, respectively. CAOB, the Central Asian Orogenic Belt; YFTB, the Yanshan Fold and Thrust Belt.

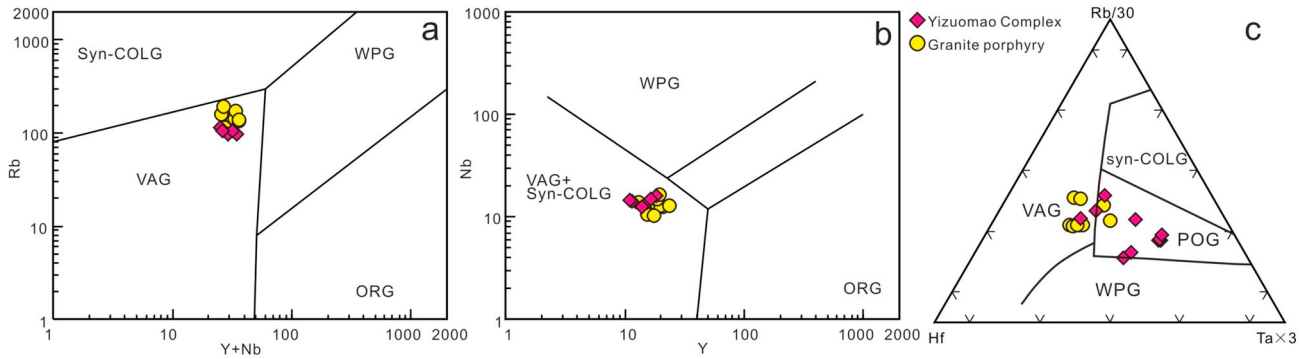

Fig. 12. Rb–(Y + Nb) (a), Nb–Y (b) and (Rb/30)–Hf–Ta × 3 (c) diagrams for samples analyzed during this study (a and b after Pearce et al., 1984, c after Harris et al., 1986). Plutonic: FG—fractionated M-, I- & S-type felsic granites; OGT—unfractionated M-, I- & S-type felsic granites; M-type granite: mantle-derived granite; I-type granite: igneous protolith granite; S-type granite: sedimentary protolith granite. ORG—ocean ridge granite; VAG—volcanic arc granite; syn-COLG—syn-collision granite; WPG—within-plate granite; POG—post-collisional granites.

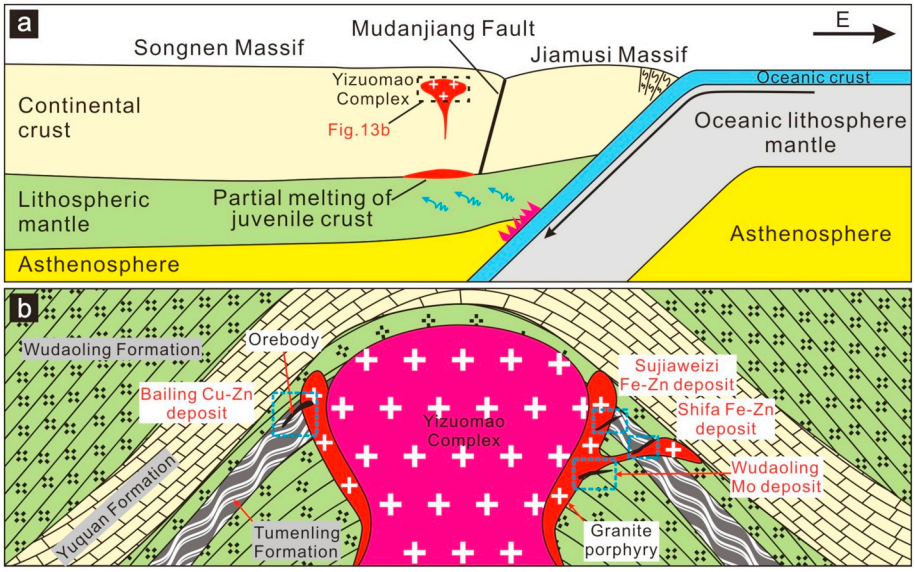

Fig. 13. A schematic plate tectonic model illustrating geodynamic evolution of Yizuomao area (a), and model of magmatism and mineralization in the Yizuomao area (b).

(mean = 8.26 and 11.29, respectively; Table 1), Zr/Hf (mean = 24.15 and 32.37, respectively), and Th/U ratios (mean = 6.38 and 3.46, respectively), which are close to average crustal compositions (Nb/Ta = 11, Zr/Hf = 33, and Th/U = 4; Taylor and Mclennan, 1985), suggesting a crustal origin for the magmas. In addition, silicic magmas with such high SiO_2 concentrations (> 63 wt%) cannot be generated by the differentiation of mantle-derived mafic magmas. This interpretation is supported by the positive $\varepsilon_{Hf}(t)$ values of the zircons, which vary between the values of CHUR and depleted mantle (Fig. 9). Therefore, we conclude that the Yizuomao Complex and granite porphyries originated from juvenile crust-derived magmas, which different from the depleted mantle fairly recently. Moreover, the skarn-forming dykes and non-mineralized Yizuomao Complex have been derived from the same protolith. Different degrees of fractionation would have been required to produce the variety of exposed granitoids, which could have been produced by varying degrees of partial melting of the crustal protolith. The $\delta^{34}S$ values of sulphides from the Bailing Cu–Zn, Wudaoling Mo and Shifa Fe–Zn deposits are 2.2–3.1‰, 3.3–3.7‰, and −0.2–4.4‰, respectively (Jiang and Li, 2012; Tan, 2009; Tan, 2013). The relatively narrow range of $\delta^{34}S$ values suggest the sulphur was derived from a unique source, possibly granitic magma. However, a granite porphyry from the Wudaoling Fe–Mo deposit has an $^{87}Sr/^{86}Sr$ ratio of 0.723123 (Xi et al., 2016), indicating that it represents a highly evolved crust-derived magma. These results indicate that the granite porphyries were derived from the partial melting of juvenile crust, which resulted from the underplating of mantle-derived magma.

6.3. Tectonic setting

The aforementioned petrogenetic and geochemical signatures suggest that the Yizuomao Complex and granite porphyries are high-K calc-alkaline rocks, with enrichment in LILEs (e.g., Rb, Th, U, K, and Pb) and depletion in Nb, Ta, P and Ti. High-K calc-alkaline I-type granites can be generated in continental arc or post-collision extensional settings (e.g., Altherr et al., 2000; Karsli et al., 2010; Pitcher, 1987; Roberts and Clemens, 1993; Topuz et al., 2010). Plotting the trace and REE data of the intrusive bodies on tectonic discrimination schemes may elucidate the origin of their magmatic sources.

Previous studies on the chronology, petrology, and geochemistry of granitoids in the eastern part of the CAOB have indicated that the post-collision extension of the NCC and the Jiamusi-Khanka Massif during the Late Paleozoic-Early Mesozoic (Shao et al., 1997; Wu et al., 2004), and the transformation of the Paleo-Asian tectonic system into the circum-Pacific tectonic system occurred after the Late Triassic (Xu et al., 2009). Furthermore, LA–ICP–MS zircon U–Pb dating indicates that the Yizuomao Complex formed at the Late Triassic to Early Jurassic. We consider that the Yizuomao Complex formed in a post-collisional extensional environment. According to the Rb, Nb, Yb, Hf, and Ta contents in the diagrams of Pearce et al. (1984) and Harris et al. (1986), the analyzed rock samples from the Yizuomao Complex all plot within the post-collision field (Fig. 12a and b). However, the most of analyzed samples plot within the post-collision field in Fig. 12c. In summary, we propose that the Yizuomao Complex formed in the transformation period from the post-collision extension of the NCC and the Jiamusi-Khanka Massif to the subduction of Paleo-Pacific Plate.

Since the Jurassic, NE China has been affected mainly by circular-Pacific tectonics and forms part of the huge circular-Pacific metallogenic belt (Wu et al., 2011a, 2011b; Zeng et al., 2012; Zhou et al., 2013; Xu et al., 2013). Mesozoic magmatism and associated metallogenesis in NE China was related to westward subduction of the Pacific Plate (Natal'in and Borukayev, 1991; Wakita and Metcalfe, 2005; Zhou et al., 2009; Hu et al., 2014), which resulted in the generation of widespread granitoids in the Lesser Xing'an Range-Zhangguangcai Range and the formation of several medium to large mineral deposits (e.g., Luming, Huojihe, Cuiling, Xiaoxilin, Xulaojiugou, and Wudaoling). This is consistent with the tectonic discrimination diagrams of Rb vs Y + Nb (Fig. 12a) and Nb vs Y (Fig. 12b), in which the analyzed samples all plot within the volcanic arc field. The eastern Asian continental margin evolved in a subduction-related tectonic setting since at least the Early Jurassic (Wakita and Metcalfe, 2005; Wu et al., 2007c). Therefore, we infer that the granite porphyries around the Yizuomao Complex formed as result of westward subduction of the Pacific Plate (Fig. 13a and b).

Thus, we conclude that the Yizuomao Complex was formed in the transformation period from the post-collision extension of the NCC and the Jiamusi-Khanka Massif to the subduction of Paleo-Pacific Plate. The granite porphyries associated with mineralization were the result of magmatic activity along an active continental margin that was related to subduction of the Paleo-Pacific Plate.

7. Conclusions

Based on new geochemical data, zircon Lu–Hf isotopic compositions,

and zircon U–Pb ages of the Yizuomao Complex and granite porphyries in the eastern Ha'erbin, we draw the following conclusions.

(1) LA–ICP–MS zircon U–Pb dating shows that the Yizuomao Complex was emplaced in the Late Triassic to Early Jurassic (195.3–205.2 Ma). The mineralization in the Yizuomao area was closely associated with the emplacement of granite porphyries within the Yizuomao Complex. The skarn mineralization likely developed during the Early to Middle Jurassic.
(2) Petrographic, geochronological, Hf isotopic, and whole-rock geochemical data suggest that the Yizuomao Complex and granite porphyries represent highly fractionated I-type granites that were derived from partial melting of juvenile crust.
(3) The Yizuomao Complex formed in the transformation period from the post-collision extension of the NCC and the Jiamusi-Khanka Massif to the subduction of Paleo-Pacific Plate, whereas the granite porphyries formed due to westward subduction of the Pacific Plate.

Acknowledgements

This study was financially supported by the China Geological Survey Program (Grants 121201103000150060) and National Natural Science Foundation of China (Grant No. 41602066). We thank the staff of the State Key Laboratory of Geological Processes and Mineral Resources, China University of Geosciences, Wuhan, China. In particular, we express our gratitude to two reviewers for their critical reviews and excellent suggestions job on improvement of the manuscript.

References

Altherr, R., Holl, A., Hegner, E., Langer, C., Kreuzer, H., 2000. High-potassium, calc-alkaline I-type plutonism in the European Variscides: northern Vosges (France) and northern Schwarzwald (Germany). Lithos 50, 51–73.
Amelin, Y., Lee, D.C., Halliday, A.N., Pidgeon, R.T., 1999. Nature of the Earth's earliest crust from hafnium isotopes in single detrital zircons. Nature 399, 252–255.
Anderson, T., 2002. Correction of common lead in U–Pb analyses that do not report ^{204}Pb. Chem. Geol. 192, 59–79.
Barbarin, B., 1996. Genesis of the two main types of peraluminous granitoids. Geology 24, 295–298.
Belousova, E.A., Griffin, W.L., O-Reilly, S.Y., Fisher, N.I., 2002. Igneous zircon: trace element composition as an indicator of source rock type. Contrib. Mineral. Pertrol. 143, 602–622.
Blichert-Toft, J., Albarède, F., 1997. The Lu–Hf isotope geochemistry of chondrites and the evolution of the mantle-crust system. Earth Planet. Sci. Lett. 148, 243–258.
Bo, J.W., Yang, Y.C., Li, Q., Ma, X.Y., Han, S.J., 2016. Formation age and tectonic setting of ore-forming rock body in Bailing copper-zinc deposit, Heilongjiang Province. Mineral Deposits 35, 225–244 (in Chinese with English abstract).
Boynton, W.V., 1984. Cosmochemistry of the Rare Earth Elements: Meteorite Studies, Rare Earth Element Geochemistry. Elsevier, Amsterdam, pp. 63–114.
Cawthorn, R.G., Brown, P.A., 1976. A model for the formation and crystallization of corundum-normative calc-alkaline magmas through amphibole fractionation. J. Geol. 84, 467–476.
Chappell, B.W., 1999. Aluminium saturation in I- and S-type granites and the characterization of fractionated haplogranites. Lithos 46, 535–551.
Chappell, B.W., White, A.J.R., 1974. Two contrasting granite types. Pac. Geol. 8, 173–174.
Chappell, B.W., Bryant, C.J., Wyborn, D., 2012. Peraluminous I-type granites. Lithos 153, 142–153.
Chen, B., Jahn, B.M., Tian, W., 2009. Evolution of the Solonker suture zone: constraints from zircon U–Pb ages, Hf isotopic ratios and whole-rock Nd–Sr isotope compositions of subduction and collision-related magmas and forearc sediments. J. Asian Earth Sci. 34, 245–257.
Chu, N.C., Taylor, R.N., Chavagnac, V., Nesbitt, R.W., Boella, R.M., Milton, J.A., German, C.R., Bayon, G., Burton, K., 2002. Hf isotope ratio analysis using multi-collector inductively coupled plasma mass spectrometry: an evaluation of isobaric interference corrections. J. Anal. Atom. Spectrosc. 17, 1567–1574.
Clemens, J.D., 2003. S-type granitic magmas–petrogenetic issues, models and evidence. Earth Sci. Rev. 61, 1–18.
Compiling Group, 1983. National Isotope Geological Age Data Collection (Third Episode). Geological Publishing House, Beijing, pp. 168–169 (in Chinese).
Frost, B.R., Barnes, C.G., Collins, W.J., Arculus, R.J., Ellis, D.J., Frost, C.D., 2001. A geochemical classification for granitic rocks. J. Petrol. 42, 2033–2048.
Gao, J.F., Lu, J.J., Lan, M.Y., Lin, Y.P., Pu, W., 2003. Analysis of trace elements in rock samples using HRICPMS. J. Nanjing Univ. (Natural Sciences) 39, 844–850 (in Chinese with English abstract).
Han, S.J., 2013. Research on Magmatic Fluids and Gold Mineralization of the Late Mesozoic Epithermal Gold System in the Northern Lesser Xing'an Range (Doctoral dissertation). Jilin University (120 p. (in Chinese with English abstract)).
Harris, N.B., Pearce, J.A., Tindle, A.G., 1986. Geochemical characteristics of collision-zone magmatism. Geol. Soc. Lond. Spec. Publ. 19, 67–81.
Hou, K.J., Li, Y.H., Zou, T.R., Qu, X.M., Shi, Y.R., Xie, G.Q., 2007. Laser ablation-MC-ICP-MS technique for Hf isotope microanalysis of zircon and its geological applications. Acta Petrol. Sin. 23, 2595–2604 (in Chinese with English abstract).
Hu, X.L., Ding, Z.J., He, M.C., Yao, S.Z., Zhu, B.P., Shen, J., Chen, B., 2014. A porphyry-skarn metallogenic system in the Lesser Xing'an Range, NE China: implications from U–Pb and Re–Os geochronology and Sr–Nd–Hf isotopes of the Luming Mo and Xulaojiugou Pb–Zn deposits. J. Asian Earth Sci. 90, 88–100.
Jahn, B.M., Windley, B., Natal'in, B., Dobretsov, N., 2004. Phanerozoic continental growth in Central Asia. J. Asian Earth Sci. 23, 599–603.
Jiang, F., Li, H., 2012. Geological characteristics and ore-controlling factors of Bailing Cu-Zn deposit. Mod. Min. 516, 41–43 (in Chinese with English abstract).
Karsli, O., Dokuz, A., Uysal, I., Aydin, F., Chen, B., Kandemir, R., Wijbrans, J., 2010. Relative contributions of crust and mantle to generation of Campanian high-K calc-alkaline I-type granitoids in a subduction setting, with special reference to the Harşit Pluton, eastern Turkey. Contrib. Mineral. Petrol. 160, 467–487.
Le Bas, M.J., Le Maitre, R.W., Streckeisen, A., Zanettin, B., 1986. A chemical classification of volcanic rocks based on the total alkali–silica diagram. J. Petrol. 27, 745–750.
Le Maitre, R.W., 1989. A Classification of Igneous Rocks and Glossary of Terms: Recommendations of the IUGS Commission on the Systematics of Igneous Rocks. 34 Blackwell Scientific Publications, Oxford.
Li, J.Y., 2006. Permian geodynamic setting of Northeast China and adjacent regions: closure of the Paleo-Asian Ocean and subduction of the Paleo-Pacific Plate. J. Asian Earth Sci. 26, 207–224.
Li, Z.T., Zhao, C.J., 1991. The Formation and Evolution of Granite Belt in Xiaoxing'anling-Zhangguangcai. Geological Publishing House, Beijing, pp. 66–75 (in Chinese).
Li, J.Y., Niu, B.G., Song, B., Xu, W.X., Zhang, Y.H., Zhao, Z.R., 1999. Crustal Formation and Evolution of Northern Changbai Mountains, Northeast China. Geological Publishing House, Beijing, pp. 32–50 (in Chinese with English abstract).
Li, X.H., Li, W.X., Li, Z.X., 2007a. On the genetic classification and tectonic implications of the Early Yanshanian granitoids in the Nanling Range, South China. Chin. Sci. Bull. 52, 1873–1885.
Li, X.H., Li, Z.X., Li, W.X., 2007b. U–Pb zircon, geochemical and Sr–Nd–Hf isotopic constrains on age and origin of Jurassic I- and A-type granites from Central Guangdong, SE China: a major igneous event in response to foundering of a subducted flat-slab. Lithos 96, 186–204.
Li, H.Y., Yang, Y.C., Ye, S.Q., Yan, W.Q., Cai, J.H., Zhang, G.B., Wang, L., 2015. Geological and geochemical characteristics and genesis of Sujia iron polymetallic deposit in Heilongjiang Province. Glob. Geol. 31, 656–664.
Liu, Y.S., Hu, Z.C., Gao, S., Günther, D., Xu, J., Gao, C.G., Chen, H.H., 2008. In situ analysis of major and trace elements of anhydrous minerals by LA-ICP-MS without applying an internal standard. Chem. Geol. 257, 34–43.
Liu, Y.S., Gao, S., Hu, Z.C., Gao, C.G., Zong, K.Q., Wang, D.B., 2010. Continental and oceanic crust recycling-induced melt-peridotite interactions in the Trans-North China Orogen: U–Pb dating, Hf isotopes and trace elements in zircons of mantle xenoliths. J. Petrol. 51, 537–571.
Ludwig, K.R., 2003. User's Manual for Isoplot 3: A Geochronological Toolkit for Microsoft Excel. 4. Berkeley Geochronology Centre Special Publication, pp. 74.
Morel, M.L.A., Nebel, O., Nebel-Jacobsen, Y.J., Miller, J.S., Vroon, P.Z., 2008. Hafnium isotope characterization of the GJ-1 zircon reference material by solution and laser-ablation MC-ICPMS. Chem. Geol. 255, 231–235.
Natal'in, B.A., Borukayev, C.B., 1991. Mesozoic sutures in the southern Far East of USSR. Geotectonics 25, 64–74.
Pearce, J.A., Harris, N.B.W., Tindle, A.G., 1984. Trace element discrimination digrams for the tectonic interpretation of granitic rocks. J. Pertol. 25, 956–983.
Pitcher, W.S., 1987. Granites and yet more granites forty years on. Geol. Rundsch. 76, 51–79.
Roberts, M.P., Clemens, J.D., 1993. Origin of high-potassium, talc-alkaline, I-type granitoids. Geology 21, 825–828.
Sengör, A.M.C., Natal'In, B.A., Burtman, V.S., 1993. Evolution of the Altaid tectonic collage and Palaeozoic crustal growth in Eurasia. Nature 364, 299–307.
Shao, J.A., Mou, B.L., He, G.Q., Zhang, L.Q., 1997. The geological process of the northern region of north China in the tectonic overprinting process of Paleo-Asian and Pacific regimes. Sci. China (D) 27, 390–394 (in Chinese).
Shi, P.H., Yang, Y.C., Ye, S.Q., Han, S.J., 2012. Geological and geochemical characteristics and genesis of ferromolybdenum deposit in Wudaoling, Heilongjiang Province. Glob. Geol. 31, 262–270.
Sun, S.S., McDonough, W.F., 1989. Chemical and Isotopic Systematic Sod Ocean Basins: Implications for Mantle Composition and Processes. Geological Society of London and Blackwell Scientific Publications, London, pp. 313–345.
Sun, J.G., Han, S.J., Zhang, Y., Xing, S.W., Bai, L.A., 2012a. Diagenesis and metallogeneticmechanisms of the Tuanjiegou gold deposit from the Lesser Xing'an Range, NE China: zircon U–Pb geochronology and Lu–Hf isotopic constraints. J. Asian Earth Sci. 62, 373–388.
Sun, J.G., Zhang, Y., Xing, S.W., Zhao, K.Q., Zhang, Z.J., Bai, L.A., Ma, Y.B., Liu, Y.S., 2012b. Genetic types, ore-forming age and geodynamic setting of endogenic molybdenum deposits in the eastern edge of Xing-Meng orogenic belt. Acta Petrol. Sin. 28, 1317–1332.
Tan, C.Y., 2009. General Characteristics of the Tectonic-Metallogenic System of Main Ore Deposits in Heilongjiang Province, Northeast China (Doctoral dissertation). China University of Geosciences, Beijing (239 p. (in Chinese with English abstract)).
Tan, H.Y., 2013. Metallogenesis Series and Prospecting Assessment in Lesser Xing'an Range-Zhangguangcai Range Metallogenic Belt of Heilongjiang Province (Doctoral

dissertation). China University of Geosciences, Beijing (150 p. (in Chinese with English abstract)).
Taylor, S.R., Mclennan, S.M., 1985. The Continental Crust: Its Composition and Evolution. 312 Blackwell Scientific Publication, London.
Topuz, G., Altherr, R., Siebel, W., Schwarz, W.H., Zack, T., Hasözbek, A., Barth, M., Satir, M., Şen, C., 2010. Carboniferous high-potassium I-type granitoid magmatism in the eastern Pontides: the Gümüşhane pluton (NE Turkey). Lithos 116, 92–110.
Vertoort, J.D., Patchett, P.J., 1996. Behavior of hafnium and neodymium isotopes in the crust: constraints from Precambrian crustally derived grnites. Geochim. Cosmochim. Acta 60, 3717–3733.
Wakita, K., Metcalfe, I., 2005. Ocean plate stratigraphy in East and Southeast Asia. J. Asian Earth Sci. 24, 679–702.
Whalen, J.B., Currie, K.L., Chanppell, B.W., 1987. A-type granites: geochemical characteristics, discrimination and petrogenesis. Contrib. Mineral. Petrol. 95, 407–419.
Windley, B.F., Alexeiev, D., Xiao, W., Kröner, A., Badarch, G., 1984. Tectonic models for accretion of the Central Asian orogenic Belt. J. Geol. Soc. Lond. 164, 31–47.
Wu, F.Y., Jahn, B.M., Wilde, S.A., Lo, C.H., Yui, T.F., Lin, Q., Ge, W.C., Sun, D.Y., 2003a. Highly fractionated I-type granites in NE China (I): geochronology and petrogenesis. Lithos 66, 241–273.
Wu, F.Y., Jahn, B.M., Wilde, S.A., Lo, C.H., Yui, T.F., Lin, Q., Ge, W.C., Sun, D.Y., 2003b. Highly fractionated I-type granites in NE China (II): isotopic geochemistry and implications for crustal growth in the Phanerozoic. Lithos 67, 191–204.
Wu, F.Y., Wilde, S.A., Sun, D.Y., Zhang, G.L., 2004. Geochronology and petrogenesis of post-orogenic Cu, Ni-bearing mafic–ultramafic intrusions in Jilin, NE China. J. Asian Earth Sci. 23, 791–797.
Wu, F.Y., Yang, Y.H., Xie, L.W., Yang, J.H., Xu, P., 2006. Hf isotopic compositions of the standard zircons and baddeleyites used in U–Pb geochronology. Chem. Geol. 234, 105–126.
Wu, F.Y., Li, X.H., Yang, J.H., Zheng, Y.F., 2007a. Discussions on the petrogenesis of granites. Acta Petrol. Sin. 23, 1217–1238 (in Chinese with English abstract).
Wu, F.Y., Zhao, G.C., Sun, D.Y., Wilde, S.A., Yang, J.H., 2007b. The Hulan Group: its role in the evolution of the Central Asian Orogenic Belt of NE China. J. Asian Earth Sci. 30, 542–556.
Wu, F.Y., Yang, J.H., Lo, C.H., Wilde, S.A., Sun, D.Y., Jahn, B.M., 2007c. The Heilongjiang Group: a Jurassic accretionary complex in the Jiamusi Massif at the western Pacific margin of northeastern China. Island Arc 16, 156–172.
Wu, F.Y., Sun, D.Y., Ge, W.C., Ge, W.C., Zhang, Y.B., Grant, M.L., Wilde, S.A., Jahn, B.M., 2011a. Geochronology of the Phanerozoic granitoids in northeastern China. J. Asian Earth Sci. 41, 1–30.
Wu, F.Y., Sun, D.Y., Ge, W.C., Zhang, Y.B., Grant, M.L., Wilde, S.A., Jahn, B.M., 2011b. Geochronology of the Phanerozoic granitoids in northeastern China. J. Asian Earth Sci. 411, 1–30.
Wyborn, D., Chappell, B.W., James, M., 2001. Examples of convective fractionation in high temperature granites from the Lachlan Fold Belt. Aust. J. Earth Sci. 48, 531–541.
Xi, A.H., Wang, M.Z., Ge, Y.H., Li, B.L., Wang, Q., Zhu, Q., 2016. Geochemical characteristics and geological significance of granite porphyry in Wudaoling, Heilongjiang Province. J. Jilin Univ. (Earth Sci. Ed.) 46, 1159–1171.
Xiao, W.J., Zhang, L.C., Qin, K.Z., Sun, S., Li, J.Y., 2004. Paleozoic accretionary and collisional tectonics of the eastern Tienshan (China): implications for the continental growth of Central Asia. Am. J. Sci. 304, 370–395.
Xiao, W.J., Windley, B.F., Han, C.M., Yuan, C., Sun, M., Li, J.L., Sun, S., 2009. End Permian to mid-Triassic termination of the southern Central Asian Orogenic Belt. Int. J. Earth Sci. 98, 1189–1217.
Xu, W.L., Ji, W.Q., Pei, F.P., Meng, E., Yu, Y., Yang, D.B., Zhang, X.Z., 2009. Triassic volcanism in eastern Heilongjiang and Jilin provinces, NE China: chronology, geochemistry, and tectonic implications. J. Asian Earth Sci. 34, 392–402.
Xu, W.L., Pei, F.P., Wang, F., Meng, E., Ji, W.Q., Yang, D.B., Wang, W., 2013. Spatial-temporal relationships of Mesozoic volcanic rocks in NE China: constraints on tectonic overprinting and transformations between multiple tectonic regimes. J. Asian Earth Sci. 74, 167–193.
Yan, W.Q., Yang, F.X., 2008. Discussion on Wudaoling Molybdenum deposits geological mineralization roles by Yicuomao rock. Gold Sci. Technol. 16, 37–42 (in Chinese with English abstract).
Yang, J.H., Wu, F.Y., Shao, J., Simon, A.W., Xie, L.W., Liu, X.M., 2006. Constraints on the timing of uplift of the Yanshan Fold and Thrust Belt, North China. Earth Planet. Sci. Lett. 246, 336–345.
Yang, F.X., Duan, P.C., Yang, W.Q., Mao, A.S., Gao, S.X., 2007. The Bailing copper zinc multi-metals deposit ore controlling factors by Yizuomao Rocks in Bindong areas. Gold Sci. Technol. 15, 15–18.
Yang, Y.C., Han, S.J., Sun, D.Y., Guo, J., Zhang, S.J., 2012. Geological and geochemical features and geochronology of porphyry molybdenum deposits in the Lesser Xing'an Range-Zhangguangcai Range metallogenic belt. Acta Petrol. Sin. 28, 379–390.
Yuan, H.L., Gao, S., Liu, X.M., Li, H.M., Günther, D., Wu, F.Z., 2004. Accurate U–Pb age and trace element determinations of zircon by laser ablation inductively coupled plasma mass spectrometry. Geostand. Newslett. 28, 353–370.
Zeng, Q.D., Liu, J.M., Chu, S.X., Wang, Y.B., Sun, Y., Duan, X.X., Zhou, L.L., 2012. Mesozoic molybdenum deposits in the east Xingmeng Orogenic Belt, Northeast China: Characteristics and tectonic setting. Int. Geol. Rev. 54, 1843–1869.
Zhang, Y., 2013. Research on Characteristics of Geology, Geochemistry and Metallogenic Mechanism of the Jurassic Molybdenum Deposits in the Mid-East Area of Jilin. Doctoral dissertation. Jilin University, pp. 157 (in Chinese with English abstract).
Zhao, M.Y., 2000. An analysis on the ore-forming characteristics of nonferrous metals and noble metal sub-ore zone in Zhangguangcai Range Tieli-Yuquan metallogenic zone. Mineral. Resour. Geol. 14, 225–229 (in Chinese with English abstract).
Zhou, J.B., Wilde, S.A., Zhang, X.Z., Zhao, G.C., Zheng, C.Q., Wang, Y.J., Zhang, X.H., 2009. The onset of Pacific margin accretion in NE China: evidence from the Heilongjiang high-pressure metamorphic belt. Tectonophysics 478, 230–246.
Zhou, J.B., Cao, J.L., Zeng, W.S., Wang, B., 2013. Confirming of the Jilin-Heilongjiang high pressure metamorphic belt and its tectonic implication. Chin. Sci. Bull. 58, 2266–2270 (in Chinese with English Abstract).
Zhou, J.B., Cao, J.L., Wilde, S.A., Zhao, G.C., Zhang, J.J., Wang, B., 2014. Paleo-Pacific subduction-accretion: evidence from Geochemical and U–Pb zircon dating of the Nadanhada accretionary complex, NE China. Tectonics 33, 2444–2466.